

AD-A017 400

DAMAGE PROFILES IN SILICON AND THEIR IMPACT ON
DEVICE RELIABILITY

G. H. Schwuttke

International Business Machines Corporation

Prepared for:

Advanced Research Projects Agency

1 July 1975

DISTRIBUTED BY:

NTIS

National Technical Information Service
U. S. DEPARTMENT OF COMMERCE

ADA017400

DAMAGE PROFILES IN SILICON and THEIR IMPACT ON DEVICE RELIABILITY

328162

G. H. Schwuttke, Principal Investigator (914) 897-3140
International Business Machines Corporation
System Products Division, East Fishkill Laboratories
Hopewell Junction, New York 12533

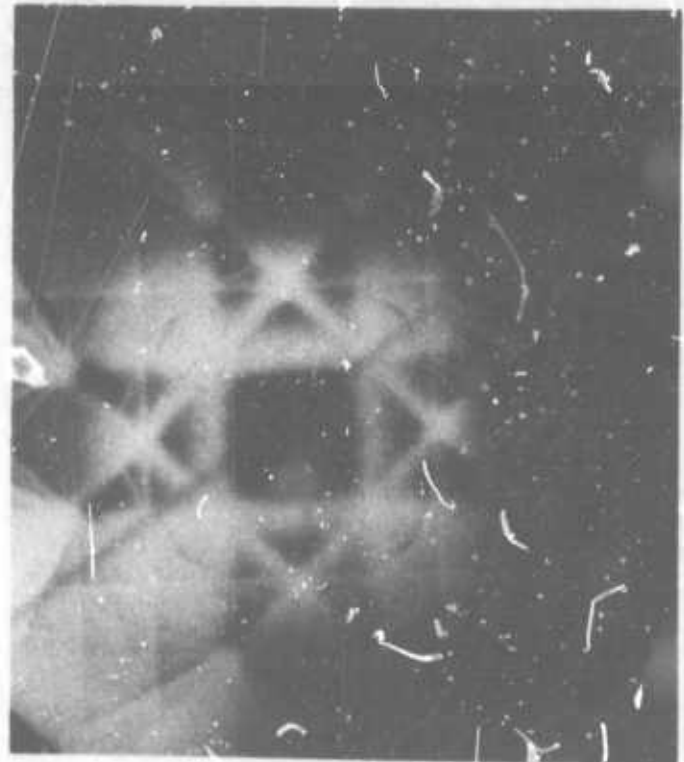
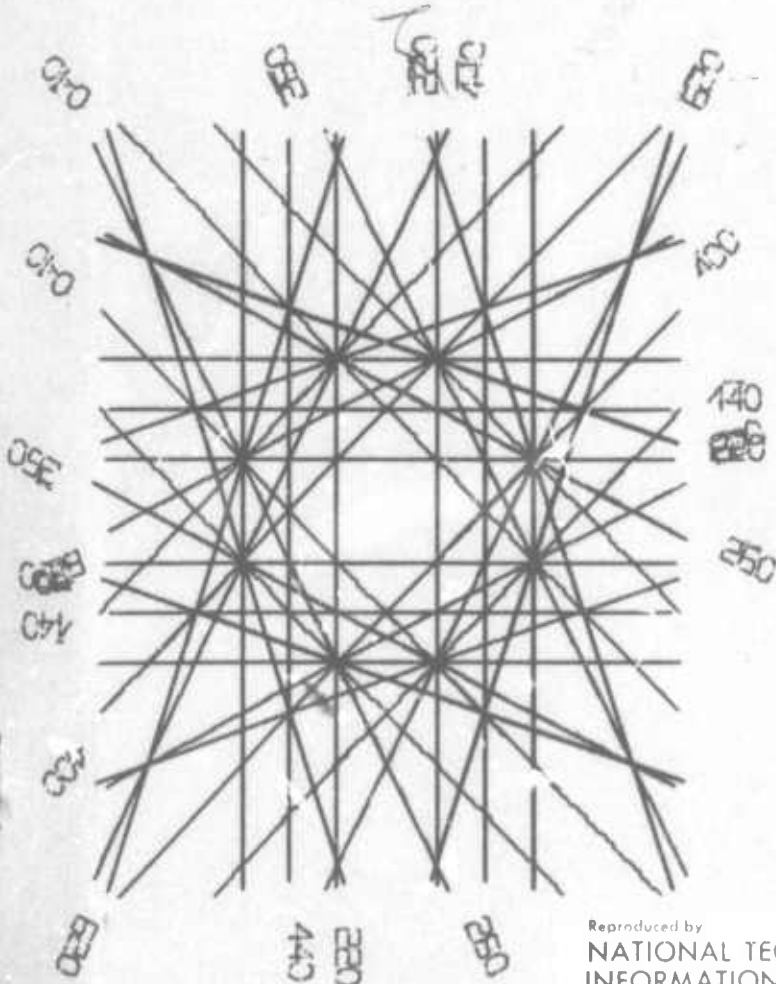
TECHNICAL REPORT No. 6
July 1975

Contract No. DAHC15-72-C-0274
Contract Monitor: Dr. C. M. Stickley

Sponsored by
Advanced Research Projects Agency
ARPA Order No. 2196, Program Code No. P2D10

DISTRIBUTION STATEMENT A

Approved for public release
Distribution Unlimited



Reproduced by
NATIONAL TECHNICAL
INFORMATION SERVICE
U S Department of Commerce
Springfield VA 22151

Kikuchi Map of (001) Silicon.
(Left) Computer generated.
(Right) Micrograph taken with
200 keV electrons.

DD
RECEIVED
SEP 18 1975
B

Unclassified

Security Classification

DOCUMENT CONTROL DATA - R&D		
<i>(Security classification of title, body of abstract and indexing annotation must be entered when the overall report is classified)</i>		
1. ORIGINATING ACTIVITY (Corporate author) International Business Machines Corporation System Products Division, East Fishkill Hopewell Junction, N. Y. 12533		2a. REPORT SECURITY CLASSIFICATION Unclassified
		2b. GROUP
3. REPORT TITLE DAMAGE PROFILES IN SILICON AND THEIR IMPACT ON DEVICE RELIABILITY		
4. DESCRIPTIVE NOTES (Type of report and inclusive dates) Scientific 1 January 1975 to 30 June 1975		
5. AUTHOR(S) (First name, middle initial, last name) G. H. Schwuttke		
6. REPORT DATE 1 July 1975	7a. TOTAL NO. OF PAGES 65	7b. NO. OF REFS 23
8a. CONTRACT OR GRANT NO. DAHC 15-72-C-0274	9a. ORIGINATOR'S REPORT NUMBER(S) TR-22.1921	
b. PROJECT, TASK, WORK UNIT NOS.		
c. OOO ELEMENT		
d. DOO SUBELEMENT	9b. OTHER REPORT NO(S) (Any other numbers that may be assigned this report)	
10. DISTRIBUTION STATEMENT		
11. SUPPLEMENTARY NOTES		12. SPONSORING MILITARY ACTIVITY Advanced Research Projects Agency
13. ABSTRACT This report summarizes investigations done during the contract period of January 1, 1975, to June 30, 1975. It describes work dealing with improvements of advanced measurement techniques. Chapter 1 deals with the computer generation of Kikuchi patterns needed for complex structural analysis of crystal defects in silicon. The program is applicable to a large variety of problems and can be used to generate Kikuchi maps for different crystal structures, each desired crystal orientation, and electron energy. The program can also be used to generate channeling patterns for scanning electron microscopy application. The report provides a complete set of computer-generated Kikuchi maps for silicon and 200 keV electrons. A complete program in Fortran IV using an IBM 1800 computer is also given. The second part describes the application of MOS C-V and MOS G-V measurements for the evaluation of epitaxial films on silicon or insulator substrates. It is shown that the presence of an underlying junction requires important precautions with use of the MOS C-V measurement technique. The junction requires an increased number of components in the equivalent network, which impedes the analysis. This chapter shows how to solve the problem. Values for MOS dot diameter, layer and substrate resistivity, oxide thickness, etc. are given and refer to ranges where meaningful lifetime measurements can be carried out.		

Unclassified

Security Classification

Unclassified

Security Classification

14.	KEY WORDS	LINK A		LINK B		LINK C	
		ROLE	WT	ROLE	WT	ROLE	WT
	Silicon Defect analysis Kikuchi patterns Transmission electron microscopy Epitaxial layers Lifetime measurements						

ia

Unclassified

Security Classification

CONTENTS	PAGE
List of Investigators	ii
Summary	iii
Chapter 1	
Computer Generation of Kikuchi Maps for Transmission Electron Microscopy (TEM) and Scanning Electron Microscopy (SEM) Investigations	
by H. Kappert	
Introduction	1
Geometry	2
Orientation	6
The Program	17
Selection of Diffraction Planes	
Transition to Desired Orientation	
Rejection of High Index and High Order Planes	
Calculation of Coordinates	
Determination of Radius and Center of Kikuchi Circle	
Provision for an (x,y) Array for the Plot	
Plotting Section	
Plotting the Pole Map	
Results	21
References	24
Appendix: Program in Fortran IV for IBM 1800 Computer	25

Chapter 2

Electrical Characterization of Quasi MOS Structures on Silicon

by W. R. Fahrner, E. F. Gorey, and C. P. Schneider

Introduction	38
Analysis of Equivalent Network	39
Spreading Resistance vs. Dot Diameter	48
Range of Quasi MOS Capacitance Technique	50
Comparison With Other Techniques	51
Results and Discussion	52
Summary and Conclusions	55
References	56

LIST OF INVESTIGATORS

The project is supervised by Dr. G. H. Schwuttke, principal investigator. The following people contributed to the work in this report:

Dr. W. Fahrner	- Investigator (Visiting Scientist)
Dr. H. Kappert	- Investigator (Visiting Scientist)
Dr. G. H. Schwuttke	- Principal Investigator
Mr. E. F. Gorey	- Technical Support
Mr. C. P. Schneider	- Technical Support
Mr. H. Ilker	- Technical Support

SUMMARY

This report summarizes work done during the contract period of January 1, 1975 to June 30, 1975. It describes research programs dealing with improvements of advanced measurement techniques. Such improvements became imperative during the course of the contract work and are needed for subsequent structural and electrical characterization of impact sound stressed (ISS'ed) silicon wafers before and after oxidation and epitaxy.

The first chapter advances the analytical capabilities of transmission electron microscopy through the application of computer-generated Kikuchi patterns. Kikuchi lines in electron diffraction patterns are used for complex crystal defect analysis based on two-beam orientation of the specimen. Since our Hitachi microscope permits seeing only about 4° of a diffraction pattern it is impossible to index Kikuchi lines without a detailed Kikuchi map. Therefore it was necessary to computer-generate Kikuchi plots. A program for the generation of such plots was written. The program was used to generate Kikuchi maps for the three main orientations (001), (011) and (111) for Si and 200 keV electrons.

An additional benefit of this computer program is that it is applicable to a large variety of problems. By changing proper parameters the same program can be used to generate maps for all kinds of crystal structures, each desired crystal orientation, electron energy, crystallographic order and maximum index-number of lines. The program considers also parameters such as map-scales and camera length of the microscope.

In addition the program can be used to compute and print out channeling patterns used for crystal orientation analysis in the scanning electron microscope. The report provides a complete set of Kikuchi maps for silicon and 200 keV electrons as well as the complete program to generate other patterns.

The second part of the report describes the application of MOS C-V measurements to the evaluation of epitaxial silicon films on silicon or insulator substrates. It is shown that the presence of a semiconductor junction under the MOS structure requires certain considerations to be made if meaningful measurements are to be obtained. The junction requires an increased number of components in the equivalent network, which impedes the analysis.

A solution to this problem is given. If one side of the junction is oxidized, a quasi MOS structure is obtained. The equivalent network of such a structure is discussed and the conditions for MOS C-V and G-V measurements are given. When the MOS admittance can be measured the following information can be obtained:

1. Surface-state density, the corresponding capture cross sections, the charge density in the oxide, and deep energy levels.
2. The doping concentration.
3. The minority carrier lifetime.

The discussion concentrates on the measurement of minority carrier lifetime in epitaxial silicon films. Values for layer and substrate resistivity, dot diameter, oxide thickness, etc., are given to establish the range for this "Quasi MOS Capacitance Technique."

Chapter 1

COMPUTER GENERATION OF KIKUCHI MAPS FOR TRANSMISSION ELECTRON MICROSCOPY (TEM) AND SCANNING ELECTRON MICROSCOPY (SEM) INVESTIGATIONS

by

H. Kappert

INTRODUCTION

Electron diffraction patterns of samples of very good crystalline perfection and of a thickness such that inelastic scattering of electrons is fairly high, show a distinct line structure superimposed on the background intensity. This line pattern is known as the Kikuchi pattern. A similar pattern (known as Coates or channeling pattern) appears in the SEM when the intensity of the backscattered electrons is recorded as an angular dependence of the incoming beam in reference to the sample orientation.

Several applications of the TEM technique such as Burgers vector determination, crystal orientation determination, and indexing of unknown spot pattern make use of such Kikuchi patterns (1-8). For such applications it is convenient to have Kikuchi maps which show the geometrical configuration of the pattern and give the indices of all lines in it.

One way to obtain such maps is to take many images in the TEM of overlapping parts of the diffraction pattern for different tilt angles of the specimen and assemble these images in a composite map. Another way is to generate plots of indexed

Kikuchi maps through a computer. The advantage of the second way is that once a program is available it is very easy to select any desired crystalline structure, sample orientation, different wavelength of electrons or even x-rays, scale of map, or order of Kikuchi lines, just by changing some parameters in the program.

To generate Kikuchi maps very good instructions can be found in the literature (4,7,9). We followed mainly the recipe given by C. T. Young and J. L. Lytton (9).

GEOMETRY

Kikuchi lines are originated by inelastically scattered electrons in the specimen. The energy losses of these electrons are small enough that they still can be considered coherent, but they have changed direction in reference to the primary electron beam. Therefore, in spite of the primary beam being off Bragg angle θ for a certain set of net planes, a particular fraction of the inelastically scattered electrons makes a Bragg reflection at these planes, e.g., (h, k, l) in Fig. 1. This can be regarded as a virtual incoming electron beam for each set of net planes, which is split below the specimen into a transmitted and a diffracted part. We find this situation not only in the plane that corresponds to the plane of the drawing in Fig. 1 but in all directions whenever the Bragg

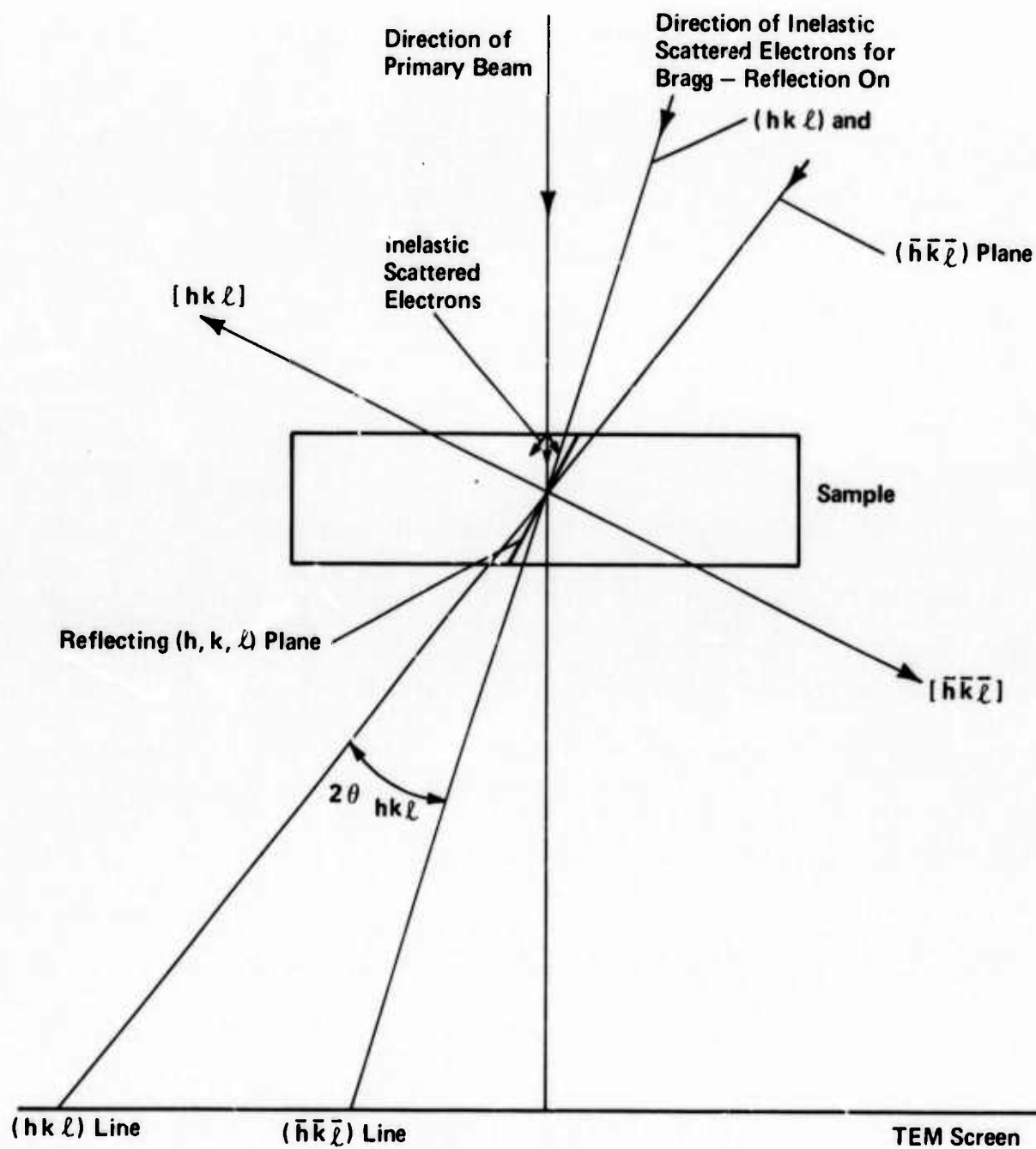


Fig. 1. Geometry for formation of Kikuchi lines.

condition is satisfied for the (h, k, l) plane. Therefore all the directions of the particular fraction of elastically scattered electrons in Bragg conditions for a certain set of net planes (h, k, l) are represented by a cone (Fig. 2), where the cone axis is in the direction of the plane normal (h, k, l) and the half opening angle is $90^\circ - \theta$ (Kossel cone). The same geometry can be used for channeling patterns in the SEM. In the SEM the primary beam itself has to be tilted along a cone surface to get a signal of the backscattered electrons with less or more intensity than for the background intensity that appears as dark or bright lines on the TV display.

The real Kikuchi line pattern is the intersection of all the cones produced by the different sets of net planes, with the image plane in the TEM below the specimen. The real channeling pattern is the intensity modulation of the backscattered electrons above the sample, as seen by the collector and displayed on the TV screen, dependent on the tilt angle of the primary beam in reference to the sample orientation.

The usual way to generate Kikuchi and channeling maps is to make a stereographic projection of all the cones, which are thus represented as circles on the projection sphere (Fig. 2). This may be done because the projection keeps the angles between intersecting lines or circles on the sphere constant, results in only small distortions of the distances especially

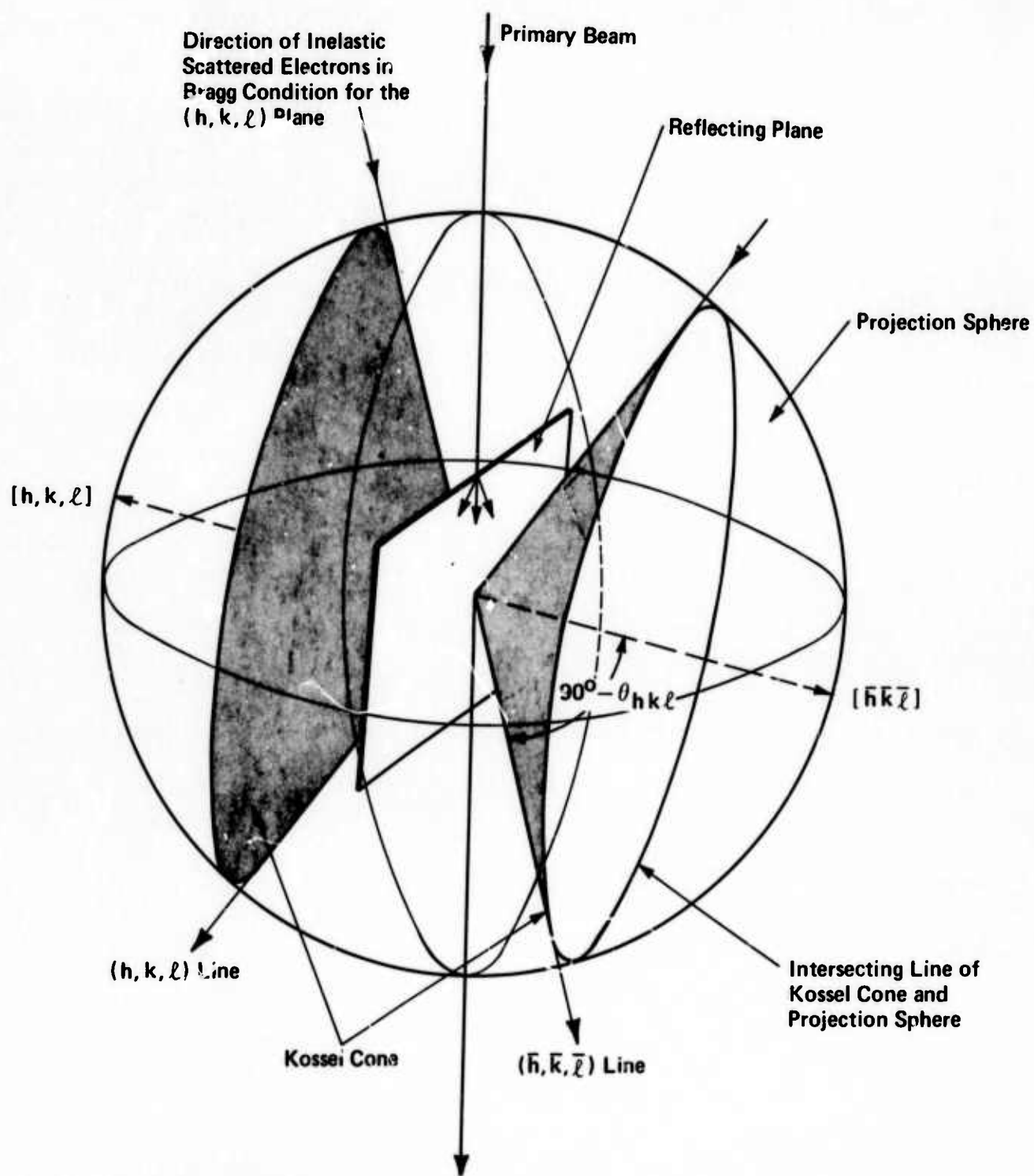


Fig. 2. Geometry of Kossel cones and their intersection with the projection sphere.

close to the center pole , and has the advantage that standard stereographic pole maps can be used for indexing purposes. The stereographic projection of the intersecting lines of the diffraction cones with the projection sphere appears as circles in the projection plane, which are called Kikuchi circles. The radius and center of each Kikuchi circle has to be calculated. Subsequently the part of the circle that is within the plotting area has to be determined and to be drawn.

ORIENTATION

Standard stereographic projections are made from G to 0 and are observed from the top, as shown in Fig. 3. The channeling patterns in the SEM are observed in the same way. To find the correct orientation between standard stereographic pole maps, channeling map and channeling pattern on the screen, we have only to consider which lenses are used to focus the primary beam onto the sample surface and how the tilt angle is related to the TV display.

The G to 0 direction of the standard stereographic projection, as shown in Fig. 3, is just the opposite to the direction in which the electrons go in the TEM to form the Kikuchi pattern on the screen. One gets around this orientation problem

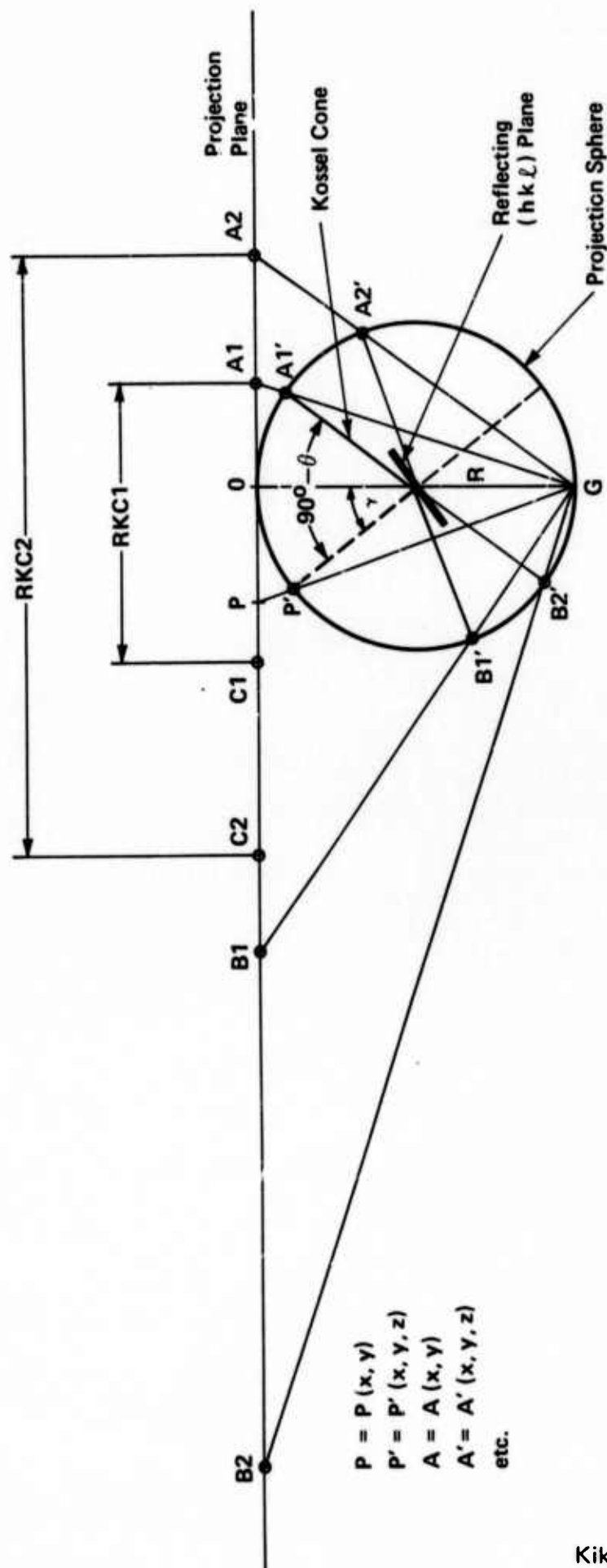


Fig. 3. Used projection and geometry to calculate radius and center of the Kikuchi circles.

by turning the projection upside down (1). Therefore standard stereographic projections have to be inverted for indexing purposes. Another possibility is to use the standard stereographic projection without inversion. This requires an adjustment of the Kikuchi maps such that the indexed reflections in the diffraction pattern correspond to the planes in the crystal. From the geometry shown in Fig. 2, one can see that the cone representing the directions of diffracted electrons intersects the projection sphere at the lower hemisphere as well as at the upper hemisphere. A downward projection--that is, the unconventional projection from O to G (Fig. 3)--would result in the real Kikuchi map as seen on the TEM screen.

An upward projection--that is, the conventional stereographic projection from G to O (Fig. 3)--results in the same map, except that this one is rotated by 180° in reference to the real Kikuchi pattern on the TEM screen. To do it this way was recently proposed by Head et al. (10). We decided to use this method because a rotation of 180° is more convenient than a mirror inversion, and we can use standard stereographic projections as in x-ray studies.

The correct orientation between the sample, the TEM micrograph, the diffraction pattern, standard pole map and Kikuchi map is found as follows:

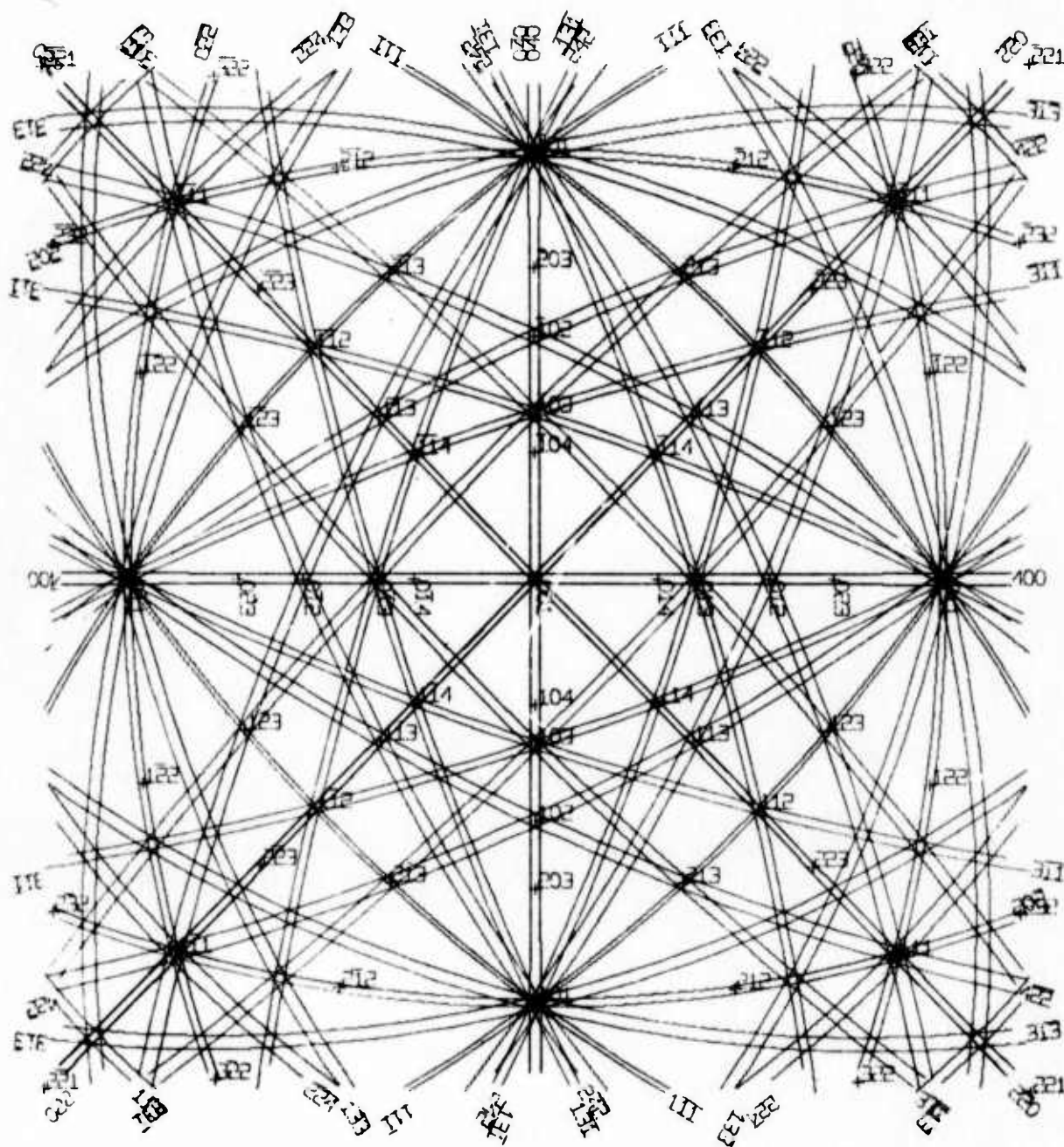
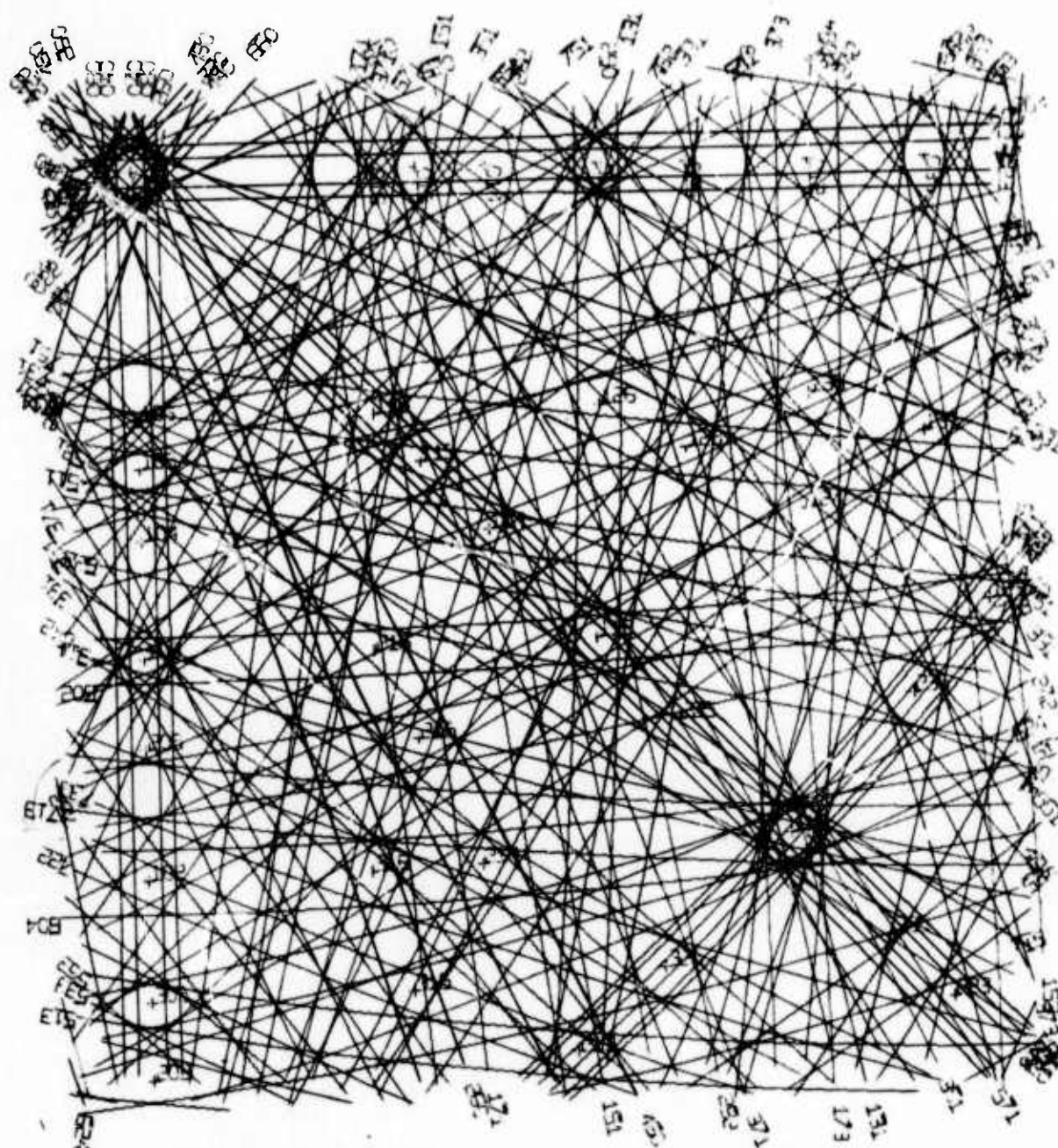


Fig. 4. (001) map for Si 200 keV, $x_0 = y_0 = 11\text{cm}$, $R = 11\text{cm}$, $\text{RMN} = 2$, $\text{SMSQ} = 5$.



Reproduced from
best available copy.



Fig. 5. (001) map for Si 200 keV, $x_c = y_o = 20\text{cm}$, $R = 32\text{cm}$, $\text{RMN} = 4$, $\text{SMSQ} = 9$.

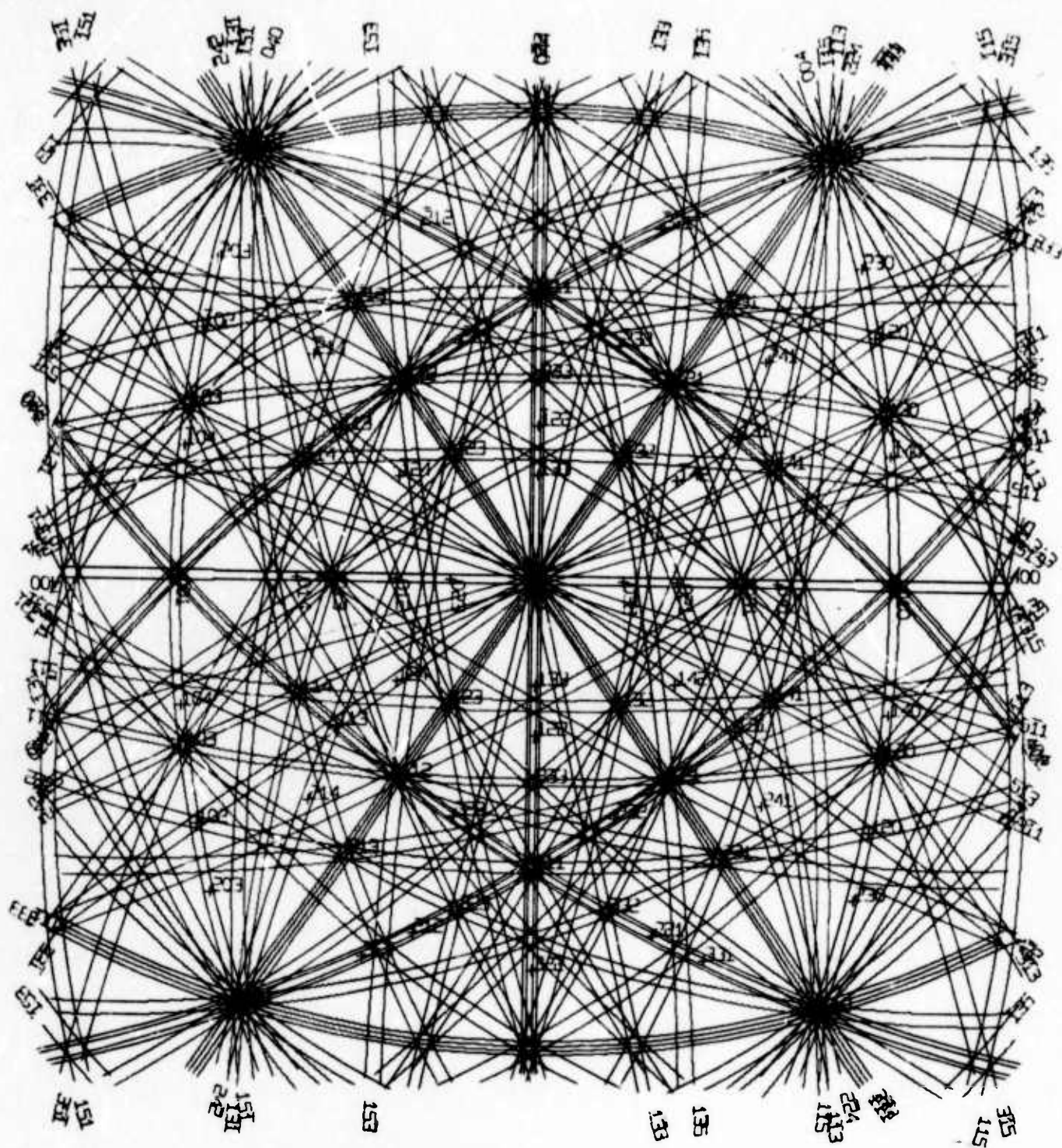


Fig. 6. (011) map for Si 200 keV, $x_0 = y_0 = 12\text{cm}$, $R = 11\text{cm}$, $\text{RMN} = 4$, $\text{SMSQ} = 5$.

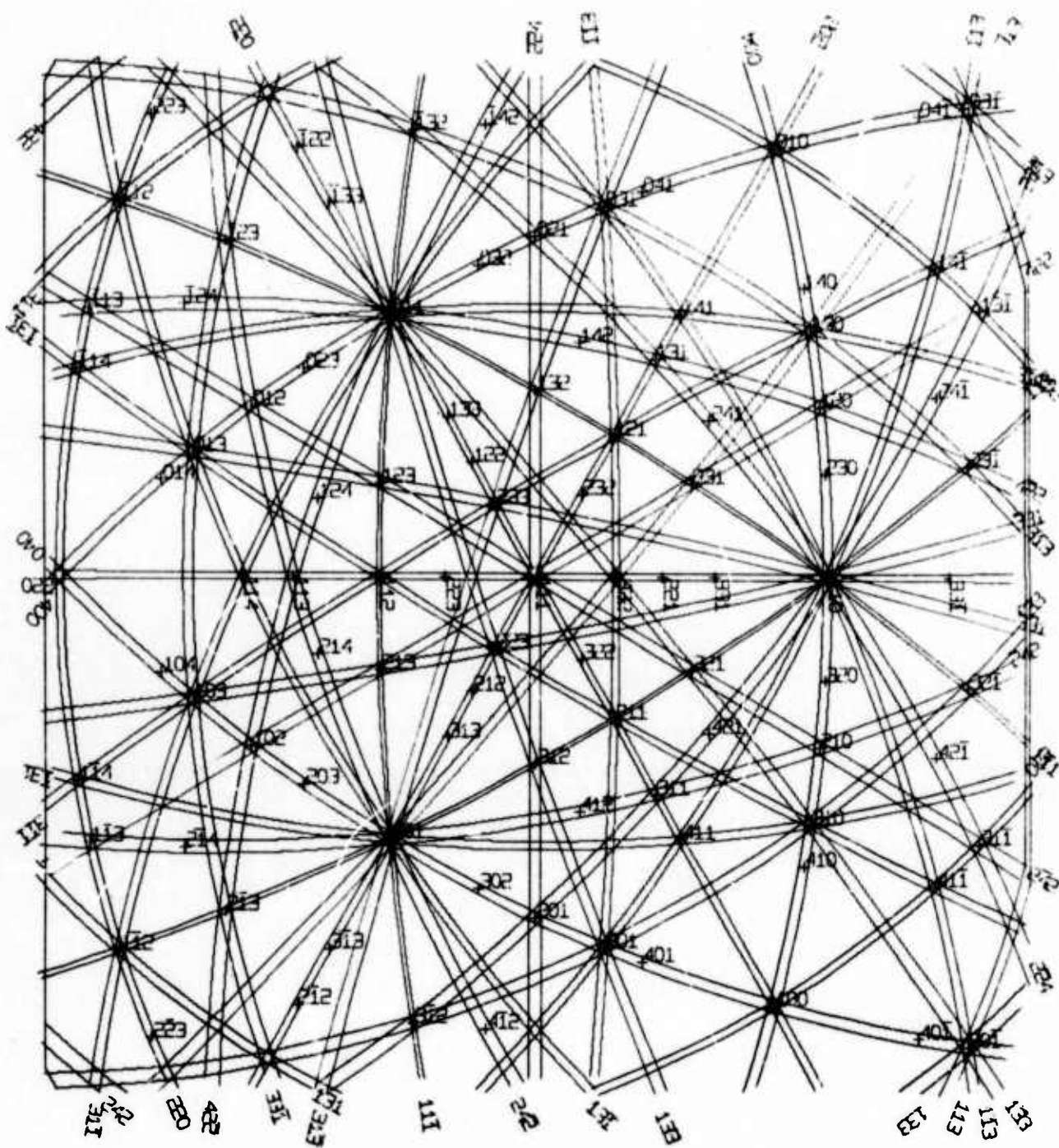


Fig. 7. (111) map for Si 200 keV, $x_0 = y_0 = 12\text{cm}$, $R = 11\text{cm}$, $\text{RMN} = 2$, $\text{SMSQ} = 5$.

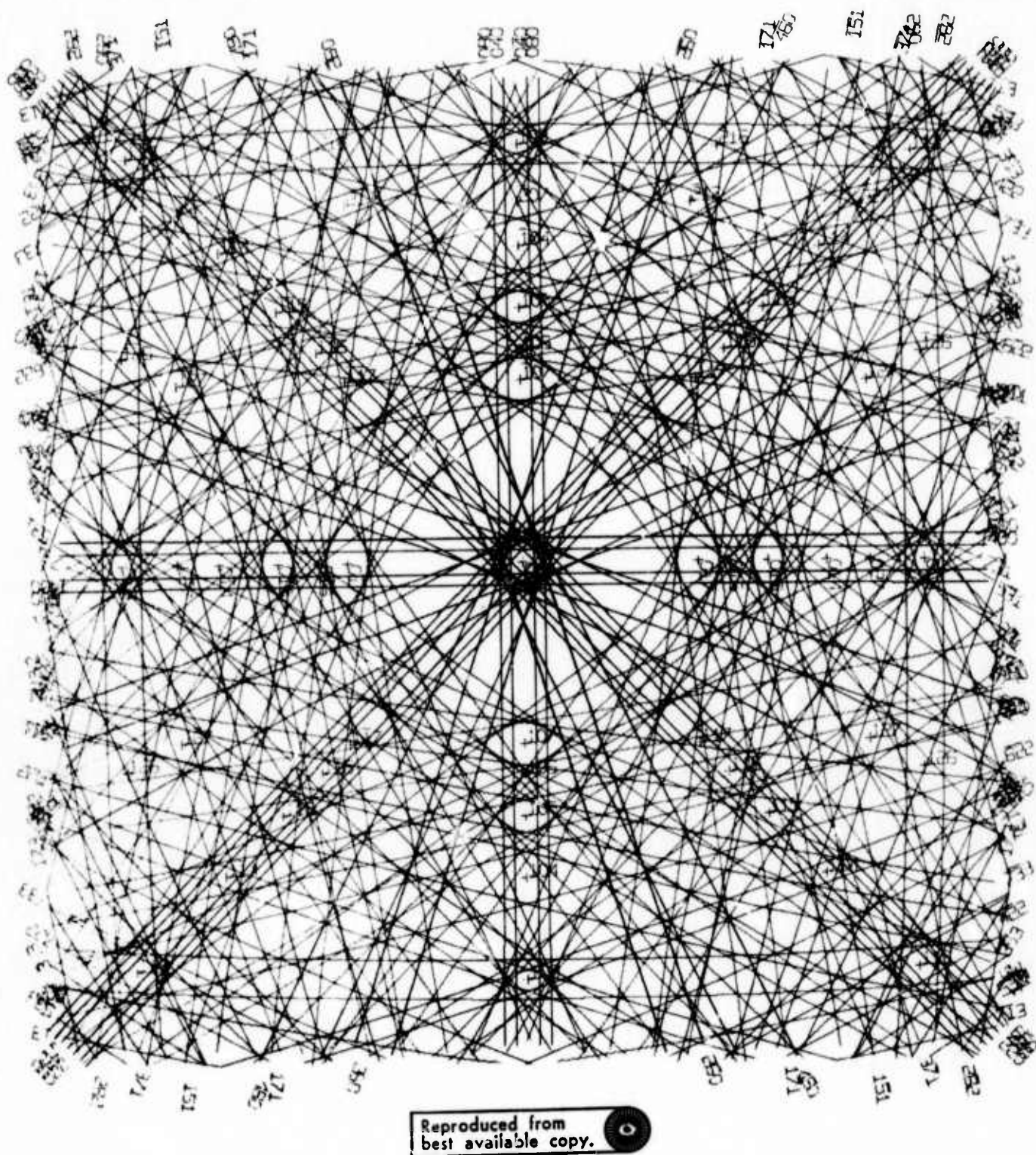


Fig. 8. (001) map for Si 200 keV, $x_0 = y_0 = 12\text{cm}$, $R = 32\text{cm}$, $\text{RMN} = 4$, $\text{SMSQ} = 9$.

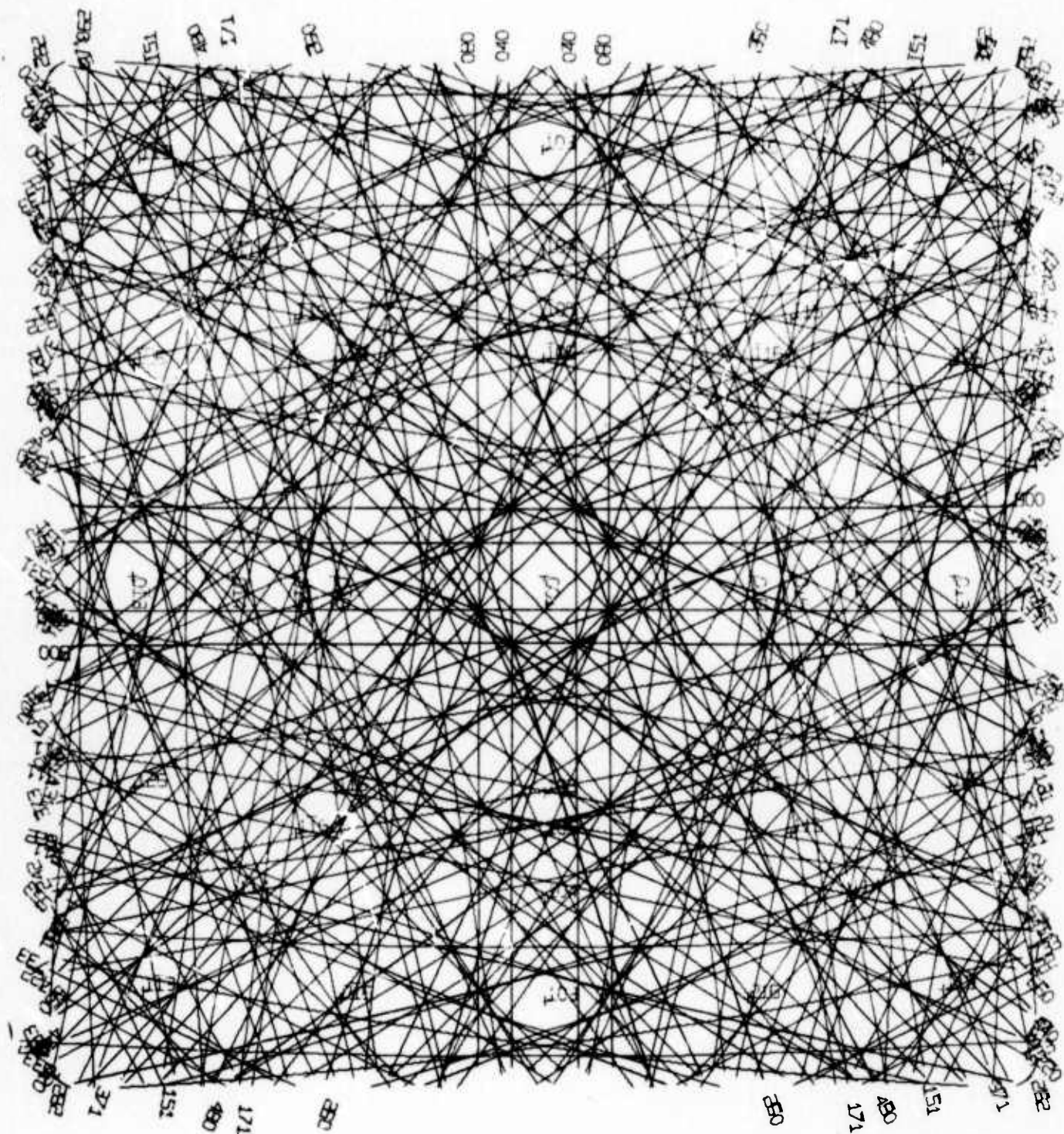


Fig. 9. (001) map for Si 30 keV, $x_0 = y_0 = 12\text{cm}$, $R = 32\text{cm}$, $\text{RMN} = 4$, $\text{SMSQ} = 9$.

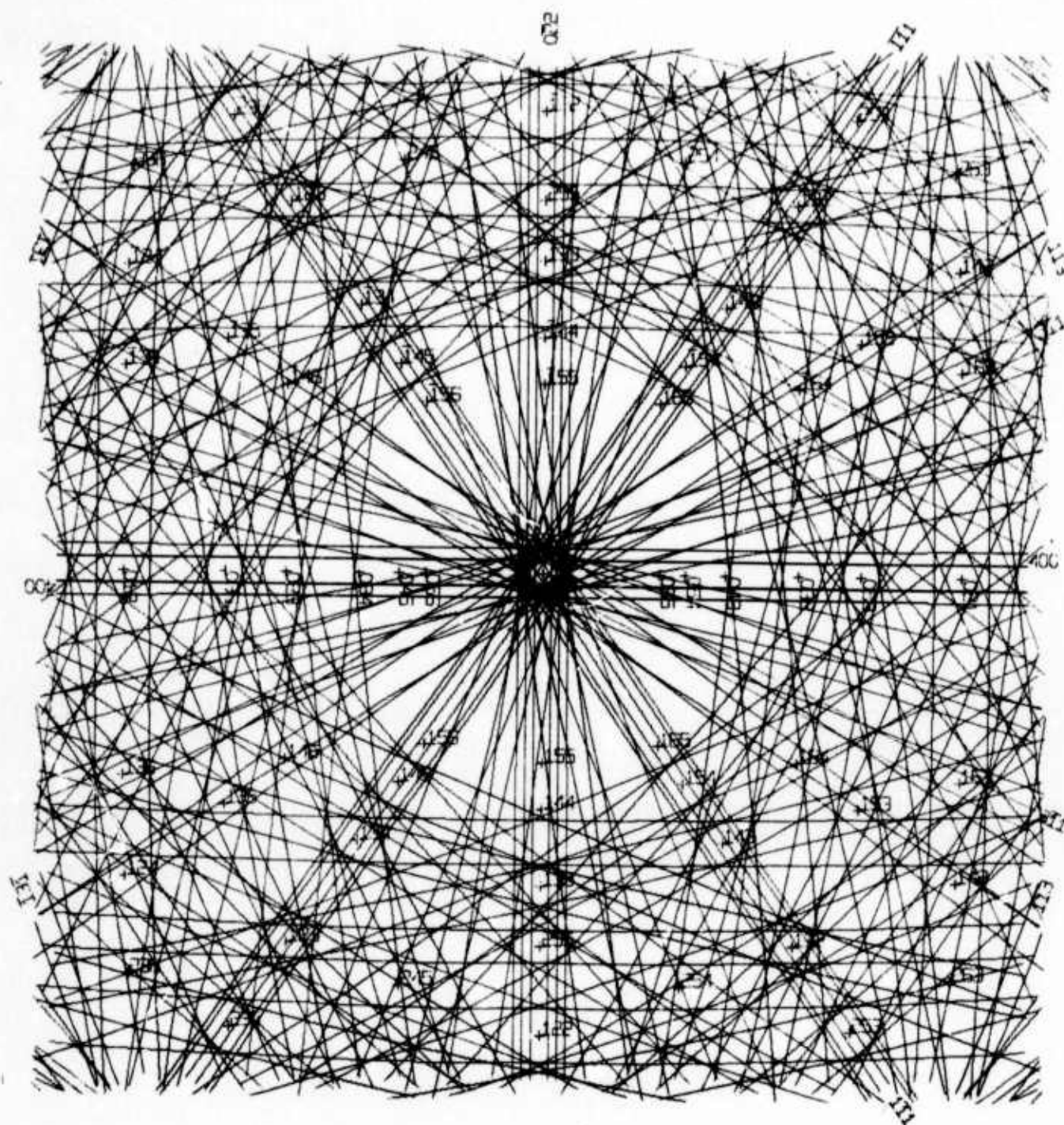


Fig. 10. (011) map for Si 200 keV, $x_0 = y_0 = 12\text{cm}$, $R = 32\text{cm}$, $\text{RMN} = 4$, $\text{SMSQ} = 9$.

Reproduced from
best available copy.

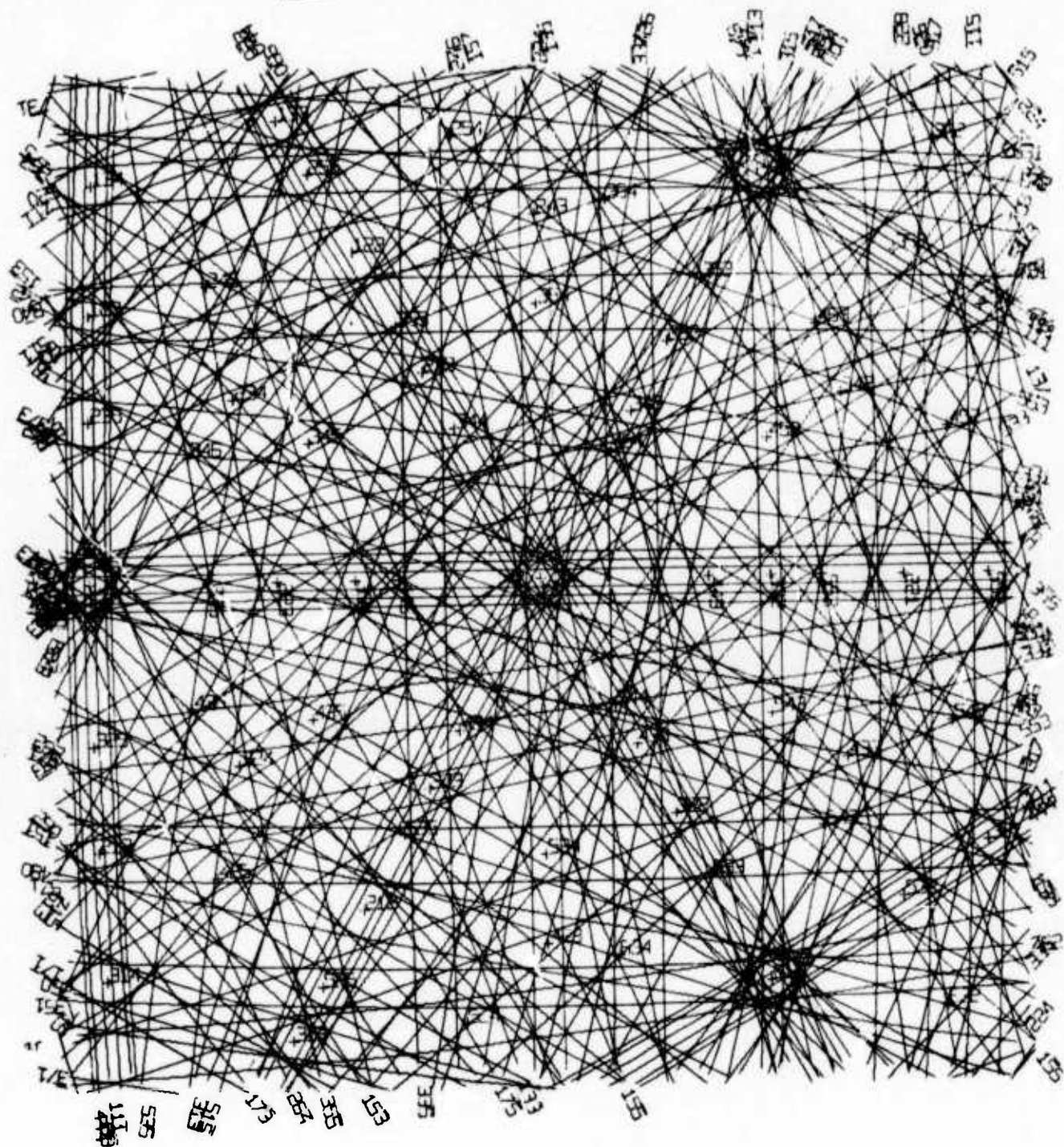


Fig. 11. (111) map for Si 200 keV, $x_0 = y_0 = 12\text{cm}$, $R = 32\text{cm}$, $\text{RMN} = 4$, $\text{SMSQ} = 9$.

1. Consider the rotation between micrograph and diffraction pattern that depends on the number of lenses used and their excitation.
2. Orient the Kikuchi plot the same way as the TEM Kikuchi pattern and take negative values of the pole indices as plotted in the map.
3. Rotate a standard stereographic pole map with the same center pole as the Kikuchi plot by 180° in reference to the pole map plotted within the Kikuchi map.

To avoid any other inversion or rotation we have to use both negatives and prints of the micrograph as recorded in the TEM on the screen.

THE PROGRAM

The program is written in Fortran IV for an IBM 1800 computer. The time used to generate one plot depends on the number of lines that have to be plotted. For example, the plot shown in Fig. 4 takes less time than the plot shown in Fig. 6, where higher order and higher index lines appear. The time for the plot in Fig. 6 was about 50 min. The attached program was used for this plot. Figures 6-11 show different plots generated with the same program when parameters used are as described in each figure caption.

Steps of the program:

1. Selection of diffraction planes

The usual structure factor equation:

$$F = \sum_{j=1}^n f_j \exp [2\pi i (u_j h + v_j k + w_j l)] \quad (1)$$

is used to calculate the structure factors for silicon so that the planes can be selected which give the Bragg reflections. For this calculation the coordinates u , v , w of the position of the 8 atoms in the Si unit cell have to be put into (1). The Bragg equation is used in the form

$$\theta_{hkl} = \frac{\lambda}{2a} \sqrt{h^2 + k^2 + l^2} = 0.0023 \sqrt{h^2 + k^2 + l^2} \quad (2)$$

for 200 keV electrons and Si samples to calculate the Bragg angles θ_{hkl} for each plane.

2. Transition to desired orientation with coordinates
X31, X32, X33

The coordinate transformation

$$\begin{pmatrix} XH \\ XU \\ XL \end{pmatrix} = \begin{pmatrix} h_1/\sqrt{s_1} & k_1/\sqrt{s_1} & l_1/\sqrt{s_1} \\ h_2/\sqrt{s_2} & k_2/\sqrt{s_2} & l_2/\sqrt{s_2} \\ h_3/\sqrt{s_3} & k_3/\sqrt{s_3} & l_3/\sqrt{s_3} \end{pmatrix} \begin{pmatrix} XHS \\ XUS \\ XLS \end{pmatrix} \quad (3)$$

is used where $(h_3, k_3, l_3) = (X_{31}, X_{32}, X_{33})$. The other vectors (h_1, k_1, l_1) and (h_2, k_2, l_2) have to be chosen in accordance with a right-handed Cartesian system.

$$s_i = h_i^2 + k_i^2 + l_i^2.$$

3. Rejection of high-index and high-order planes

Planes of high-index numbers larger than a maximum number $SMSQ = \sqrt{h^2 + k^2 + l^2}$ have to be rejected; the same is true for planes of higher order than maximum order RMN.

4. Calculation of coordinates in the projection plane

The coordinates of one intersection point of the diffraction cone with the projection sphere have to be calculated. For this purpose spherical polar coordinates are introduced. Then the calculation of the coordinates within the projection plane has to be performed by the equation

$$\begin{aligned} P_x &= 2R \tan \gamma/2 \frac{P_x'}{(P_x'^2 + P_y'^2)^{1/2}} \\ P_y &= 2R \tan \gamma/2 \frac{P_y'}{(P_y'^2 + P_y'^2)^{1/2}} \end{aligned} \quad (4)$$

where $\gamma = \cos^{-1} (P_z'/R)$, as can be seen from Fig. 3.

5. Determination of the radius and center of the Kikuchi circle

From Fig. 3 it can be deduced that the radius of the Kikuchi circle is

$$\overline{CA} = 1/2 (\overline{BO} + \overline{OA}) \quad (5)$$

and the coordinates of the circle center C are

$$CX = P_x (\overline{CO}/\overline{PO})$$

$$CY = P_y (\overline{CO}/\overline{PO})$$

6. Provision for an (x,y) array for the plot

Only a small part of the Kikuchi circle in an area with radius $RI = \text{SQRT}(XO \times XO + YO \times YO)$ around the center pole has to be plotted. Therefore it has to be checked whether a particular Kikuchi circle has a part of it inside this area. Then the circle equation

$$[X - CX]^2 + [Y - CY]^2 = R^2 = [\overline{CA}]^2 \quad (6)$$

is used to provide an array of 50 (x,y) pairs for the plotter.

7. Plotting section

A final check is made to find out which values of the array are inside the plotting square given by XO and YO. The

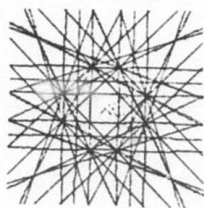
slope of the lines near the border of this square is determined in order to plot the indices of this Kikuchi line pair at the end of the line with the same slope.

8. Plotting the pole map

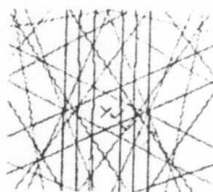
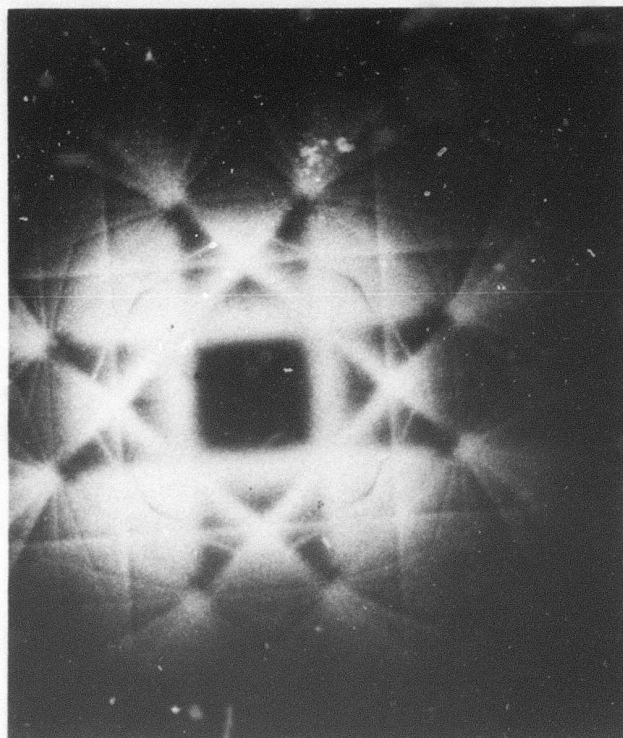
An extra program was written to produce pole maps of the same scale as the Kikuchi map. The steps are essentially similar to steps 2, 3, and 4 above.

RESULTS

The size of each plot is about $24 \times 24 \text{ cm}^2$, which is the maximum usable size of the plotter used. The numbers inside the map represent the indices of the pole where the location is indicated by a +. The numbers outside the map represent the indices of a certain Kikuchi line pair. The indices are plotted at one end of the respective Kikuchi line with the same slope as the lines at this end. Figures 4, 5, 6, and 7 represent (001), (011), and (111) Kikuchi maps with the same scale for Si with 200 keV electrons. Figures 8, 10, and 11 again represent (001), (011), and (111) Kikuchi maps for Si with 200 keV electrons but for about three times larger scale and with higher-order and higher-index lines. Figure 5 is a larger scale plot of the lower-right quadrant of Fig. 4; and Fig. 9 is the same plot as Fig. 8 but with 30 keV electrons and can be used as a map for channeling pattern for the SEM. Figure 12 gives several examples of Kikuchi poles as shown on the maps and in the TEM.



(001) pole



(114) pole

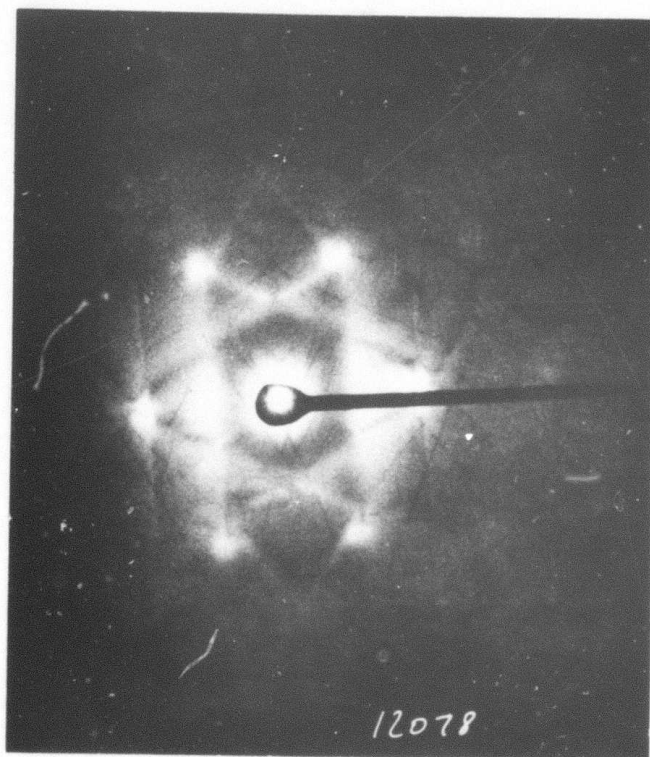
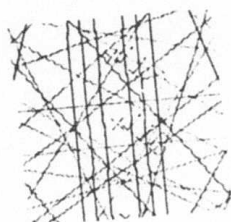
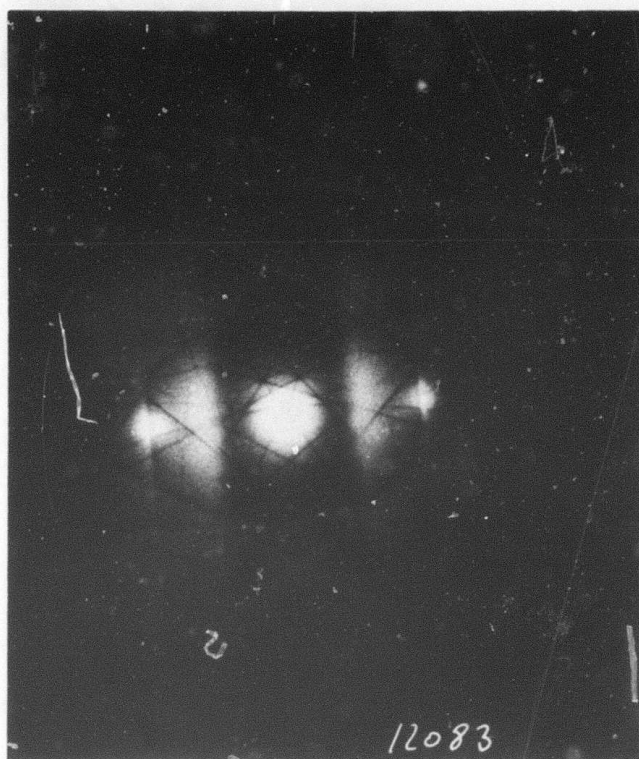


Fig. 12. Kikuchi poles of Si with 200 keV electrons as shown on the map of Fig. 5 and in the Hitachi TEM.



(116) pole



(115) pole



Fig. 12. Kikuchi poles of Si with 200 keV electrons as shown on the map of Fig. 5 and in the Hitachi TEM.

ACKNOWLEDGMENT

The author wishes to thank R. Anderson and G. Das for helpful discussions

REFERENCES

1. P. B. Hirsch et al., Electron Microscopy of Thin Crystals, Butterworths, 1965.
2. S. Amelinckx et al., Modern Diffraction and Imaging Techniques in Material Science, North Holland, 1970.
3. L. E. Murr, Electron Optical Applications in Materials Science, McGraw Hill, 1970.
4. E. Levine et al., J. Appl. Phys. 37, 2141 (1966).
5. P. R. Okamoto et al., J. Appl. Phys. 38, 289 (1967).
6. M. V. Heimendahl, Phys. Stat. Sol. (a) 5, 137 (1971).
7. J. C. Bomback and L. E. Thomas, J. Appl. Cryst. 4, 356 (1971).
8. W. K. Wu and J. Washburn, J. Appl. Phys. 45, 1085 (1974).
9. C. T. Young and J. L. Lytton, J. Appl. Phys. 43, 1408 (1972).
10. A. K. Head et al., Computed Electron Micrographs and Defect Identification, North Holland, 1973.

APPENDIX—FORTRAN IV PROGRAM

```

// JOB      Y      Z      02 JAN 70 20.331 HRS
// FOR PROG 02 JAN 70 20.331 HRS
*IOCS(CARD, 1443 PRINTER)
*IOCS (PLOTTER)
*TRANSFER TRACE
*ARITHMETIC TRACE
*LIST ALL
*ONE WORD INTEGERS
  INTEGER H,HI,H1A,HA
  DIMENSION U(8),V(8),W(8),CX(2),CY(2),RKC(2),
  1X(50),Y(50),XP(50),YP(50),SF(17,17,9)
C
C READ LATTICE PARAMETER
C
  DO 10 I=1,8
    READ (2,7) U(I),V(I),W(I)
  7 FORMAT (3F6.2)
  10 CONTINUE
C
C READ R OF STEREO SPHERE
C
  READ (2,8) R
  8 FORMAT (F6.2)
C
C R1=RAIUS OF PLOTTING CIRCLE, X0,Y0 PLOTTING SQUARE
C
  X0=12.5
  Y0=12.5
  R1=SQRT(X0*X0+Y0*Y0)
C
C PRODUCE (H,K,L) VALUES
C
  DO 19 H=1,9
    H1=H-1
    DO 29 K=1,9
      K1=K-1
      DO 39 L=1,9
        L1=L-1
      39 CONTINUE
    29 CONTINUE
  19 CONTINUE
C
C CALCULATE STRUCTURFACTOR
C
  F1=0.0
  F2=0.0
  THET=0.0
  DO 50 M=1,8
    A=6.28*(U(M)*H1+V(M)*K1+W(M)*L1)
    F1=F1+COS(A)
    F2=F2+SIN(A)
  50 CONTINUE
  F=ROUND(F1**2+F2**2)
  SF(H,K,L)=F
  39 CONTINUE
  29 CONTINUE
  19 CONTINUE
  XSCAL=0.39
  YSCAL=XSCAL
  CALL SCALF (XSCAL,YSCAL,0.0,0.0,0)
  DO 20 H=1,17

```

KIKU0000
KIKU0001
KIKU0002

KIKU0010
KIKU0012
KIKU0014
KIKU0016

KIKU0020
KIKU0022

KIKU0023
KIKU0024
KIKU0025

KIKU0050
KIKU0051
KIKU0060
KIKU0061
KIKU0070
KIKU0071

KIKU0080
KIKU0085
KIKU0090
KIKU0095
KIKU0100
KIKU0105
KIKU0106
KIKU0107
KIKU0110
KIKU0117
KIKU0118
KIKU0119
KIKU0120

KIKU5207
KIKU5208
KIKU0122

02 JAN 70
PAGE 003

XK=A21+XHS+A22+XKS+A23+XLS
XL=A31+XHS+A32+XKS+A33+XLS
IF(XL) 40,130,130

C
C REJECT PLANES OF HIGHER ORDER
C

130 Y11=10000.*(H1A-1)+100.*(K1A-1)+(L1A-1)

00 80 IH=1,5

IH1=IH-1

00 90 IK=1,5

IK1=IK-1

00 100 IL=1,5

IL1=IL-1

IF(IH1+IK1+IL1) 100,100,101

101 00 110 N=2,8

X12=N*(10000.*(IH1+100.*(IK1+IL1))

RDX1=X11-X12

ARDX=ABS(ROXI)

IF(AROX-0.1) 45,45,46

46 IF(ROXI) 100,45,110

45 00 111 M=1,8

IH5=IH1+M+1

IK5=IK1+M+1

IL5=IL1+M+1

IG=IH1+IK1+IL1

IF(IG) 111,111,43

43 FH=SF(IH5,IK5,IL5)

IF(FH-1.) 111,111,41

111 CONTINUE

41 RN=FLOAT(N)

RM=FLOAT(M)

RAN=RGUNO(RN/RM)

IF(RMN-4.) 252,252,40

110 CONTINUE

100 CONTINUE

90 CONTINUE

80 CONTINUE

C
C COORDINATES FOR DIFFR.CONE ON SPHERE
C

252 IF (XH) 253,254,255

255 A1=XK/XH

PHI=ATAN(A1)

GO TO 261

254 IF (XK) 257,256,256

256 C=0.

S=1.

GO TO 259

257 C=0.

S=-1.

GO TO 259

253 IF(XK) 258,260,258

258 A1=XK/XH

PHI=ATAN(A1)+3.141593

GO TO 261

KIKU0386
KIKU0387

KIKU0390
KIKU0391
KIKU0392
KIKU0393
KIKU0394
KIKU0395
KIKU0396
KIKU0397
KIKU0398
KIKU0399
KIKU0400
KIKU0402
KIKU0403
KIKU0404
KIKU0406
KIKU0407
KIKU0408
KIKU0409
KIKU0410
KIKU0411
KIKU0412
KIKU0413
KIKU0415
KIKU0416
KIKU0417
KIKU0418
KIKU0419
KIKU0420
KIKU0421
KIKU0422
KIKU0425

KIKU0440
KIKU0442
KIKU0444
KIKU0446
KIKU0448
KIKU0450
KIKU0451
KIKU0452
KIKU0453
KIKU0454
KIKU0455
KIKU0457
KIKU0459
KIKU0460
KIKU0461

```

260 C=-1.
S=0.
GO TO 259
261 C=COS(PHI)
S=SIN(PHI)
259 IF (XL) 265,262,263
262 TH=1.570796
GO TO 264
263 A2=SQRT((R/XL)**2-1.)
TH=ATAN(A2)
GO TO 264
265 A2=-SQRT((R/XL)**2-1.)
TH=ATAN(A2)
IF (TH) 266,266,264
266 TH=TH+3.141593
C
264 ARG12=TH+1.570796-THET
S12=SIN(ARG12)
C12=COS(ARG12)
XH12=R*C*S12
XK12=R*S*S12
XL12=R*C12
C
ARG21=TH-1.570796+THET
S21=SIN(ARG21)
C21=COS(ARG21)
XH21=R*C*S21
XK21=R*S*S21
XL21=R*C21
C
ARG11=TH+1.570796+THET
S11=SIN(ARG11)
C11=COS(ARG11)
XH11=R*C*S11
XK11=R*S*S11
XL11=R*C11
C
ARG22=TH-1.570796-THET
S22=SIN(ARG22)
C22=COS(ARG22)
XH22=R*C*S22
XK22=R*S*S22
XL22=R*C22
C
C CALCULATE COORDINATES IN PROJECTION PLANE
C FOR DIFFR. CONE
C
A12=SQRT((R/XL12)**2-1.)
IF (XL12) 271,2710,272
271 GAM12=(3.141593-ATAN(A12))/2.
GO TO 273
272 GAM12=ATAN(A12)/2.
GO TO 273
2710 GAM12=0.785398
273 TAN12=SIN(GAM12)/COS(GAM12)

```

260 C=-1.

S=0.

GO TO 259

261 C=COS(PHI)

S=SIN(PHI)

259 IF (XL) 265,262,263

262 TH=1.570796

GO TO 264

263 A2=SQRT((R/XL)**2-1.)

TH=ATAN(A2)

GO TO 264

265 A2=-SQRT((R/XL)**2-1.)

TH=ATAN(A2)

IF (TH) 266,266,264

266 TH=TH+3.141593

C

264 ARG12=TH+1.570796-THET

S12=SIN(ARG12)

C12=COS(ARG12)

XH12=R*C*S12

XK12=R*S*S12

XL12=R*C12

C

ARG21=TH-1.570796+THET

S21=SIN(ARG21)

C21=COS(ARG21)

XH21=R*C*S21

XK21=R*S*S21

XL21=R*C21

C

ARG11=TH+1.570796+THET

S11=SIN(ARG11)

C11=COS(ARG11)

XH11=R*C*S11

XK11=R*S*S11

XL11=R*C11

C

ARG22=TH-1.570796-THET

S22=SIN(ARG22)

C22=COS(ARG22)

XH22=R*C*S22

XK22=R*S*S22

XL22=R*C22

C

C CALCULATE COORDINATES IN PROJECTION PLANE

C FOR DIFFR. CONE

C

A12=SQRT((R/XL12)**2-1.)

IF (XL12) 271,2710,272

271 GAM12=(3.141593-ATAN(A12))/2.

GO TO 273

272 GAM12=ATAN(A12)/2.

GO TO 273

2710 GAM12=0.785398

273 TAN12=SIN(GAM12)/COS(GAM12)

02 JAN 70
PAGE 005

F12=2.*R*TAN12/SORT(XH12*XH12+XK12*XK12)

A1X=XH12*F12

A1Y=XK12*F12

C

A21=SQRT((R/XL21)**2-1.)

IF (XL21) 274,2740,275

274 GAM21=(3.141593-ATAN(A21))/2.

GO TO 276

275 GAM21= ATAN(A21)/2.

GO TO 276

2740 GAM21=0.785398

276 TAN21=SIN(GAM21)/COS(GAM21)

F21=2.*R*TAN21/SORT(XH21*XH21+XK21*XK21)

B1X=XH21*F21

B1Y=XK21*F21

C

A11=SQRT((R/XL11)**2-1.)

IF (XL11) 278,2780,279

278 GAM11=(3.141593-ATAN(A11))/2.

GO TO 280

279 GAM11= ATAN(A11)/2.

GO TO 280

2780 GAM11=0.785398

280 TAN11=SIN(GAM11)/COS(GAM11)

F11=2.*R*TAN11/SORT(XH11*XH11+XK11*XK11)

A2X=XH11*F11

A2Y=XK11*F11

C

A22=SQRT((R/XL22)**2-1.)

IF (XL22) 281,2810,282

281 GAM22=(3.141593-ATAN(A22))/2.

GO TO 283

282 GAM22= ATAN(A22)/2.

GO TO 283

2810 GAM22=0.785398

283 TAN22=SIN(GAM22)/COS(GAM22)

F22=2.*R*TAN22/SORT(XH22*XH22+XK22*XK22)

B2X=XH22*F22

B2Y=XK22*F22

C

C CALCULATE RADIUS AND COORDINATES OF KKC RKC1 AND RKC2

C

A8X1=B1X-A1X

A8Y1=B1Y-A1Y

ARX2=B2X-A2X

ABY2=B2Y-A2Y

C

RKC(1)=0.5*SQRT(ABX1*ABX1+ABY1*ABY1)

CX(1)=(A1X+B1X)/2.

CY(1)=(A1Y+B1Y)/2.

C

RKC(2)=0.5*SQRT(ABX2*ABX2+ABY2*ABY2)

CX(2)=(A2X+B2X)/2.

CY(2)=(A2Y+B2Y)/2.

WRITE (5,6968) H1,K1,L1,RKC(1),CX(1),CY(1),RKC(2),CX(2),CY(2)

KIKU0620
KIKU0625
KIKU0630

KIKU0635
KIKU0636
KIKU0637

KIKU0638
KIKU0639
KIKU0641

KIKU0643
KIKU0645
KIKU0648

KIKU0650
KIKU0655

KIKU0660
KIKU0661
KIKU0662

KIKU0663
KIKU0664
KIKU0666

KIKU0668
KIKU0670
KIKU0675

KIKU0680
KIKU0685

KIKU0690
KIKU0691
KIKU0692

KIKU0693
KIKU0694
KIKU0695

KIKU0698
KIKU0700
KIKU0705

KIKU0710
KIKU0715

KIKU0720
KIKU0725
KIKU0730

KIKU0735
KIKU0755
KIKU0760

KIKU0765
KIKU0770
KIKU0775

KIKU0780

6968 FORMAT (2X,3I3,2X,6F12.2)

C
C CHECK INTERSECTION OF PLOT CIRCLE WITH KC
C

DO 500 I=1,2
SCH=.5*(R1*R1+CX(I)*CX(I)+CY(I)*CY(I)-RKC(I)*RKC(I))
R11=CX(I)*CX(I)+CY(I)*CY(I)
SCH1=(CY(I)-CY(I)*R1-R1-SCH*SCH)/R11+(SCH*CX(I)/R11)**2
IF (SCH1) 401,410,410
401 SCH2=SCH1+5.E-5
IF (SCH2) 40,410,402
402 SCH1=0.0

C
C CALCULATE INTERSECTION
C

410 SQS=SQRT(SCH1)
X1=SCX*CX(I)/R11+SQS
X2=SCX*CX(I)/R11-SQS
Y1=SQRT(R1-R1-X1*X1)
Y2=SQRT(R1-R1-X2*X2)
Y1=RKC(I)-SQRT((X1-CX(I))**2+(Y1-CY(I))**2)
Y2=RKC(I)-SQRT((X1-CX(I))**2+(Y1-CY(I))**2)
T1A=ABS(T1)
IF (T1A-0.01) 430,430,420
420 Y1=-Y1
430 T2=RKC(I)-SQRT((X2-CX(I))**2+(Y2-CY(I))**2)
T2A=ABS(T2)
IF (T2A-0.01) 441,441,440
440 Y2=-Y2
GO TO 450
441 RY=ABS(Y1-Y2)-0.1
IF (RY) 449,449,450
449 Y2=-Y2
450 X15=X1-CX(I)
X25=X2-CX(I)
Y15=Y1-CY(I)
Y25=Y2-CY(I)
IF (X15) 505,510,515
515 IF (Y15) 517,516,516
516 ALF1=ATAN(Y15/X15)
GO TO 528
517 ALF1=ATAN(Y15/X15)+6.283186
GO TO 528
510 IF (Y15) 520,523,526
526 ALF1=1.570796
GO TO 528
523 ALF1=0.
GO TO 528
520 ALF1=4.712389
GO TO 528
505 ALF1=ATAN(Y15/X15)+3.141593
528 IF (X25) 525,530,535
535 IF (Y25) 537,536,536
536 ALF2=ATAN(Y25/X25)
GO TO 5450
537 ALF2=ATAN(Y25/X25)+6.283186

KIKU0810
KIKU0820
KIKU0823
KIKU0830
KIKU0840
KIKU0841
KIKU0842
KIKU0843

KIKU0850
KIKU0860
KIKU0870
KIKU0880
KIKU0890
KIKU0900
KIKU0901
KIKU0902
KIKU0920
KIKU0930
KIKU0931
KIKU0940
KIKU0950
KIKU0952
KIKU0954
KIKU0956
KIKU0958
KIKU0960
KIKU0970
KIKU0980
KIKU0990
KIKU0982
KIKU0983
KIKU0984
KIKU0985
KIKU0986
KIKU0987
KIKU0988
KIKU0990
KIKU0992
KIKU0994
KIKU0995
KIKU0996
KIKU0997
KIKU0999
KIKU1000
KIKU1001
KIKU1002
KIKU1003
KIKU1004

02 JAN 70
PAGE 007

KIKU1005
KIKU1006
KIKU1008
KIKU1009
KIKU1010
KIKU1011
KIKU1013
KIKU1015
KIKU1017

KIKU4999
KIKU5000
KIKU5002
KIKU5004
KIKU5005
KIKU5006
KIKU5010
KIKU5020
KIKU5030
KIKU5040
KIKU5050
KIKU5060
KIKU5075
KIKU5110
KIKU5120
KIKU5200

KIKU5210

KIKU5220
KIKU5230
KIKU5240

KIKU5310
KIKU5312
KIKU5314
KIKU5316
KIKU5318
KIKU5320
KIKU5328
KIKU5330
KIKU5335
KIKU5340

```
GO TO 5450
530 IF(Y2S) 540,543,546
546 ALF2=1.57
GO TO 5450
543 ALF2=0.
GO TO 5450
540 ALF2=4.712389
GO TO 5450
525 ALF2=ATAN(Y2S/X2S)+3.141593
5450 IF(X1S) 5451,5451,5452
5452 IF(X2S) 5451,5451,5453
5453 IF(Y1S) 5455,5451,5454
5454 IF(Y2S) 5456,5451,5451
5456 ALF2=ALF2-6.283186
GO TO 5451
5455 IF(Y2S) 5451,5451,5458
5458 ALF1=ALF1-6.283186
5451 DALF=(ALF1-ALF2)/50.
J=0
DO 600 M1=1,50
IF(H1)5501,5501,5502
5501 M=M1
GO TO 5503
5502 M=51-M1
5503 X(M)=RKC(I)*COS(ALF1-DALF*(M-1))+CX(I)
Y(M)=RKC(I)*SIN(ALF1-DALF*(M-1))+CY(I)
AX=ABS(X(M))
AY=ABS(Y(M))
IF(XO-AX) 600,550,550
550 IF(YO-AY) 600,580,580
580 J=J+1
XP(J)=X(M)
YP(J)=Y(M)
600 CONTINUE
C
C PLOTTING SECTION
C
IF(J-2) 500,699,699
699 CALL FPLLOT (-2,XP(1),YP(1))
WRITE(5,6962) H,K,L
6962 FORMAT (8X,313)
DO 700 JJ=1,J
700 CALL FPLLOT (0,XP(JJ),YP(JJ))
CALL FPLLOT (-1,XP(J),YP(J))
IF(I-1) 500,500,7000
7000 DY=YP(J)-YP(J-2)
DX=XP(J)-XP(J-2)
IF(DX) 7012,7011,7010
7010 DEL=ATAN(DY/DX)
GO TO 7020
7011 DEL=0.0
GO TO 7020
7012 DEL=ATAN(DY/DX)+3.141593
7020 XB=XP(J)+0.5*COS(DEL)
YB=YP(J)
```

```

HA=IABS(H1)
KA=IABS(K1)
LA=IABS(L1)
CALL FCHAR(X8,Y8,.1,.12,DEL)
WRITE(11,7099) HA,KA,LA
7099 FORMAT (3I1)
XB1=X8-0.35*SIN(DEL)
YB1=Y8+0.35*COS(DEL)
DXB=0.25*COS(DEL)
DYB=0.25*SIN(DEL)
XB2=XB1+DXB
YB2=YB1+DYB
XB3=XB1+2.*DXB
YB3=YB1+2.*DYB
XB4=XB1+3.*DXB
YB4=YB1+3.*DYB
IF(H1) 7061,7060,7060
7061 CALL FPLT(-2,XB1,YB1)
CALL FPLT(-1,XB2,YB2)
7060 IF(K1) 7071,7070,7070
7071 CALL FPLT(-2,XB2,YB2)
CALL FPLT(-1,XB3,YB3)
7070 IF(L1) 7081,40,40
7081 CALL FPLT(-2,XB3,YB3)
CALL FPLT(-1,XB4,YB4)
500 CONTINUE
40 CONTINUE
30 CONTINUE
20 CONTINUE
CALL EXIT
END

```

KIKU5341
KIKU5342
KIKU5343
KIKU5345
KIKU5350
KIKU5351
KIKU5360
KIKU5361
KIKU5362
KIKU5363
KIKU5365
KIKU5366
KIKU5367
KIKU5368
KIKU5369
KIKU5370
KIKU5372
KIKU5374
KIKU5375
KIKU5376
KIKU5377
KIKU5378
KIKU5379
KIKU5380
KIKU5381
KIKU5382
KIKU5400
KIKU5500
KIKU5600

VARIABLE ALLOCATIONS

VIR)=001E-0010	WIR)=002E-0020	CXIR)=0032-0030	CYIR)=0036-0034	RKCIR)=003A-0033
YIR)=0102-00A0	XP(R)=0166-0104	YP(R)=01CA-0168	SF(R)=161C-01CC	R(R)=161E
YOR)=1622	RIR)=1624	FLR)=1626	F2(R)=1628	THET(R)=162A
FIR)=162E	XSCAL(R)=1630	YSCAL(R)=1632	SO(R)=1634	SMSO(R)=1636
XKSIR)=163A	XL5(R)=163C	X11(R)=163E	X12(R)=1640	X13(P)=1642
X22(R)=1646	X23(R)=1648	X31(R)=164A	X32(R)=164C	X33(R)=164E
S2(R)=1652	S3(R)=1654	A11(R)=1656	A12(R)=1658	A13(R)=165A
A22(R)=165E	A23(R)=1660	A31(R)=1662	A32(R)=1664	A33(R)=1666
XK(R)=166A	XL(R)=166C	X11(R)=166E	X12(R)=1670	RDX1(R)=1672
FHR)=1676	PNR)=1678	RM(R)=167A	RMN(R)=167C	A1(R)=167E
CIR)=1682	SIR)=1684	THR)=1686	A2(R)=1688	ARG12(R)=168A
C12(R)=168E	XH12(R)=1690	XK12(R)=1692	XL12(R)=1694	ARG21(R)=1696
C21(R)=169A	XH21(R)=169C	XK21(R)=169E	XL21(R)=16A0	ARG11(R)=16A2
C11(R)=16A6	XH11(R)=16A8	XK11(R)=16AA	XL11(R)=16AC	ARG22(R)=16AE
C22(R)=16B2	XH22(R)=16B4	XK22(R)=16B6	XL22(R)=16B8	GAM12(R)=16BA
F12(R)=16BE	A1X(R)=16C0	AIY(R)=16C2	GAM21(R)=16C4	TAN21(R)=16C6
B1Y(R)=16CC	B1Y(R)=16CC	TAN22(R)=16CE	TAN11(R)=16D0	F11(R)=16D2
A2Y(R)=16D6	GAM22(R)=16D8	TAN22(R)=16DA	F22(R)=16DC	B2X(R)=16DE
ABX1(R)=16E2	ABY1(R)=16E4	ABX2(R)=16E6	ABY2(R)=16E8	SCH(R)=16EA
SCH1(R)=16EE	SCH2(R)=16F0	SOS(R)=16F2	X1(R)=16F4	X2(R)=16F6
Y2(R)=16FA	T1(R)=16FC	T1A(R)=16FE	T2(R)=1700	T2A(R)=1702
X1S(R)=1706	X2S(R)=1708	Y1S(R)=170A	Y2S(R)=170C	AI(R)=170E

```

ALF2(R) =1710
DEL(R) =171C
DYB(R) =1728
Y84(R) =1734
K(I) =1745
LIA(I) =1748
IL1(I) =1751
J(I) =1757

DALF(R) =1712
X8(R) =171E
X82(R) =172A
H(I) =1740
K1(I) =1746
IH(I) =174C
N(I) =1752
M1(I) =1758

AX(R) =1714
Y8(R) =1720
Y82(R) =172C
H1(I) =1741
L(I) =1747
IH1(I) =174D
IH5(I) =1753
JJ(I) =1759

AY(R) =1716
XB1(R) =1722
XB3(R) =172E
H1A(I) =1742
L1(I) =1748
IK(I) =174E
IK5(I) =1754
KA(I) =175A

OY(R) =1718
YB1(R) =1724
YB3(R) =1730
HA(I) =1743
M(I) =1749
IK1(I) =174F
IL5(I) =1755
LA(I) =1758

DX(4) =171A
DX8(R) =1726
XB4(R) =1732
I(I) =1744
K1A(I) =174A
IL(I) =1750
IG(I) =1756

```

STATEMENT ALLOCATIONS

```

7 =179E 8 =17A1 6968 =17A3 6962 =17AA 7099 =17AE 10 =17C4 50 =184A 39 =1873 29 =187C 19 =1885
60 =18E3 140 =1917 141 =191E 130 =1A2C 101 =1A70 46 =1AA4 45 =1AA8 43 =1AD7 111 =1AE8 41 =1AF
110 =1812 100 =1818 90 =1824 80 =182D 252 =1836 255 =183D 254 =184A 256 =184F 257 =1859 253 =1864
258 =1869 260 =1878 261 =1883 259 =188D 262 =1894 263 =189A 265 =1880 266 =188A 264 =18CA 264 =18D0 271 =1C26
272 =1C91 2710 =1C9A 273 =1C9E 274 =1CE9 275 =1CE3 283 =1DC7 401 =1EE4 402 =1EEF 410 =1EF5 420 =1F6C 430 =1F71
280 =1064 281 =1DAF 282 =1DRA 2810 =1FC0 450 =1FC5 515 =1FEF 516 =1FF4 517 =2001 510 =2010 526 =2017 523 =2010
440 =1FA7 441 =1FAE 449 =1FC0 450 =1FC5 515 =1FEF 516 =1FF4 517 =2001 510 =2010 526 =2017 523 =2010
520 =2023 505 =2029 528 =2036 535 =2030 536 =2042 537 =204F 530 =205E 546 =2065 543 =2068 540 =207
525 =2077 5450 =2084 5455 =208E 5454 =2095 5456 =209A 5455 =20A2 5458 =20A7 5451 =20AD 5501 =20C2
5502 =20C8 5503 =20CE 550 =212D 580 =2134 600 =2152 699 =2162 700 =2188 7000 =21D7 7010 =21FC 7011 =2209
7012 =220F 7020 =221C 7061 =22A3 7060 =22B7 7071 =228C 7081 =22D0 7081 =22D5 500 =22E9 40 =22F2 30 =22F8
20 =2304

```

FEATURES SUPPORTED
TRANSFER TRACE
ARITHMETIC TRACE
ONE WORD INTEGERS
IOCS

CALL SUBPROGRAMS

FSORT	FCOS	FSIN	ROUND	SCALF	IABS	FABS	FATAN	FLOT	FCHAR	FAOD	FADOX	FSUB	FSUBX	FMFY
FMPYX	FDIV	FLO	FLDX	FSTO	FSBR	FSBRX	FQVR	FAXI	MVAR	MFARX	MIAR	FLOAT	MIIF	MFIF
MRED	MVRT	MCOMP	MIOFX	MIOF	MIOI	SUBSC	SNR	FCHRI	MOLEB	PRNTN	EBPRT	CARDN		

REAL CONSTANTS

```

.25000E 02=1760
.50000E 01=176C
.314159E 01=1778
.628318E 01=1784
.25000E 00=1790
.00000E 00=1762
.50000E 00=176E
.157079E 01=177A
.471239E 01=1786
.30000E 01=1792
.628000E 01=1764
.100000E 05=1770
.20000E 01=177C
.157000E 01=1788
.390000E 00=1766
.100000E 03=1772
.785398E 00=177E
.500000E 02=178A
.100000E 01=1768
.100000E 00=1774
.500000E 04=1780
.120000E 00=178C
.230000E 02=176A
.400000E 01=1776
.100000E 01=1782
.350000E 00=178E

```

INTEGER CONSTANTS

```

1=1794 8=1795 2=1796 9=1797 17=1798 5=1799 0=179A 50=1798 51=179C 11=179D

```

CORE REQUIREMENTS FOR PROG
COMMON 0 INSKEL COMMON 0
VARIABLES 5984 PROGRAM 2992

END OF COMPILATION


```

// FOR PROG 02 JAN 70 20.079 HRS
*JOCS(CARD, 1443 PRINTER)
*JOCS (PLOTTER)
*TRANSFER TRACE
*ARITHMETIC TRACE
*LIST ALL
*ONE WORD INTEGERS
  INTEGER HZ,HZ1,HZ11,MZA
C
C  RADIUS R OF PROJ. SPHERE
C
  R=11.
  XSCAL=0.39
  YSCAL=XSCAL
  CALL SCALF(XSCAL,YSCAL,0.0,0.0)
C
C  SIZE OF MAP 2*X0*2*Y0 CM*CM
C
  X0=11.
  Y0=11.
  DO 300 HZ=7,17
    HZ1=HZ-9
    DO 310 KZ=7,17
      KZ1=KZ-9
      DO 320 LZ=7,17
        LZ1=LZ-9
        SQ=SQRT(FLOAT(HZ1*HZ1+KZ1*KZ1+LZ1*LZ1))
      C
      C  REJECT HIGH INDEX POLES
      C
      SMSQ=4.
      IF(SMSQ-SQ) 320,320,329
      329 IF(SQ-0.5) 320,320,351
      351 FZ=R/SQ
      XHZS=HZ1*FZ
      XKZS=KZ1*FZ
      XLZS=LZ1*FZ
    C
    C  TRANSITION TO DESIRED ORIENTATION WITH COORD. X31,X32,X33
    C
    X11=1.
    X12=0.
    X13=0.
    X21=0.
    X22=1.
    X23=-1.
    X31=0.
    X32=1.
    X33=1.
    S1=SQRT(X11*X11+X12*X12+X13*X13)
    S2=SQRT(X21*X21+X22*X22+X23*X23)
    S3=SQRT(X31*X31+X32*X32+X33*X33)
    A11=X11/S1
    A12=X12/S1
    A13=X13/S1
    A21=X21/S2
    A22=X22/S2
    A23=X23/S2

```

KIKU6000

KIKU5901
KIKU5902
KIKU5000
KIKU6010
KIKU6020
KIKU6030
KIKU6040
KIKU6041
KIKU6045

KIKU6046
KIKU6047
KIKU6048
KIKU6049
KIKU6050
KIKU6051
KIKU6052

KIKU6055
KIKU6056
KIKU6057
KIKU6058
KIKU6059
KIKU6060
KIKU6061
KIKU6062
KIKU6063
KIKU6065
KIKU6066
KIKU6067
KIKU6068
KIKU6069
KIKU6070
KIKU6071
KIKU6072
KIKU6073

mf

02 JAN 70
PAGE 002

A31=X31/S3
A32=X32/S3
A33=X33/S3
XHZ=A11*XHZS+A12*XKZS+A13*XLZS
XKZ=A21*XHZS+A22*XKZS+A23*XLZS
XLZ=A31*XHZS+A32*XKZS+A33*XLZS
IF (XLZ) 320,301,301

C
C REJECT HIGH ORDER POLES
C

301 HZA=IABS(HZ1)
KZA=IABS(KZ1)
LZA=IABS(LZ1)
X11=10000.*HZA+100.*KZA+LZA
DO 340 IH=1,5
IH1=IH-1
DO 341 IK=1,5
IK1=IK-1
DO 342 IL=1,5
IL1=IL-1
DO 343 N=2,8
IF (IH1+IK1+IL1) 344,342,344
344 X12=N*(10000.*IH1+100.*IK1+IL1)
RX1=X11-X12
IF (RX1) 342,320,343
343 CONTINUE
342 CONTINUE
341 CONTINUE
340 CONTINUE

C
C CALCULATE COORD. IN PROJECTION PLANE
C

AZ=SQRT((R/XLZ)**2-1.)
IF (XLZ) 354,353,352
354 GAMZ=(3.14193-ATAN(AZ))/2.
GO TO 356
352 GAMZ=ATAN(AZ)/2.
GO TO 356
353 GAMZ=0.785398
356 TANZ=SIN(GAMZ)/COS(GAMZ)
SORA=SQRT(XHZ*XHZ+XKZ*XKZ)
IF (SORA-0.5) 359,359,355
355 FZ1=2.*R*TANZ/SORA
PXZ=XHZ*FZ1
PYZ=XKZ*FZ1
GO TO 358
359 AXLZ=ARS(XLZ)
IF (AXLZ-0.5) 320,320,357
357 PXZ=0.0
PYZ=0.0
358 APXZ=ABS(PXZ)
APYZ=ABS(PYZ)

C
C SLECT POLES WITHIN THE PLOTTED AREA
C

KIKU6074
KIKU6075
KIKU6076
KIKU6080
KIKU6081
KIKU6082
KIKU6085

KIKU6090
KIKU6052
KIKU6053
KIKU6054
KIKU6055
KIKU6056
KIKU6057
KIKU6058
KIKU6059
KIKU6060
KIKU6061
KIKU6062
KIKU6063
KIKU6064
KIKU6064
KIKU6065
KIKU6066
KIKU6067
KIKU6068

KIKU6110
KIKU6112
KIKU6114
KIKU6116
KIKU6118
KIKU6120
KIKU6122
KIKU6130
KIKU6135
KIKU6138
KIKU6140
KIKU6150
KIKU6160
KIKU6162
KIKU6164
KIKU6166
KIKU6168
KIKU6169
KIKU6170
KIKU6171

PAGE 003

```

IF(XO-APXZ) 320,321,321
321 IF(YO-APYZ) 320,324,324
C
C PLOT + AND NUMBER (HZ1,KZ1,LZ1) AT COORDINATES (PXZ,PYZ)
C
324 CALL FPLOT (-2,PXZ,PYZ)
CALL POINT (0)
CALL FPLOT (-1,PXZ,PYZ)
HZ1=IABS(HZ1)
KZ1=IABS(KZ1)
LZ1=IABS(LZ1)
IF(APXZ-0.1) 326,326,325
325 CALL FCHAR (PXZ-0.06*XSCAL,PYZ+0.1*YSCAL,.1,.12,1.571)
WRITE (11,390) HZ1,KZ1,LZ1
390 FORMAT (311)
IF(HZ1) 361,360,360
361 CALL FPLOT (-2,PXZ-0.40,PYZ+0.04)
CALL FPLOT (-1,PXZ-0.40,PYZ+0.24)
360 IF (KZ1) 371,370,370
371 CALL FPLOT (-2,PXZ-0.40,PYZ+0.25)
CALL FPLOT (-1,PXZ-0.40,PYZ+0.50)
370 IF (LZ1) 381,320,320
381 CALL FPLOT (-2,PXZ-0.40,PYZ+0.55)
CALL FPLOT (-1,PXZ-0.40,PYZ+0.80)
GO TO 320
326 CALL FCHAR(PXZ+0.06*XSCAL,PYZ+0.1*YSCAL,.1,.12,0.0)
WRITE(11,391)HZ1,KZ1,LZ1
391 FORMAT(311)
IF(HZ1)366,365,365
366 CALL FPLOT(-2,PXZ+0.03,PYZ+0.4)
CALL FPLOT(-1,PXZ+0.24,PYZ+0.4)
365 IF(KZ1)376,375,375
376 CALL FPLOT(-2,PXZ+0.25,PYZ+0.4)
CALL FPLOT(-1,PXZ+0.50,PYZ+0.4)
375 IF(LZ1)386,320,320
386 CALL FPLOT(-2,PYZ+0.55,PYZ+0.4)
CALL FPLOT(-1,PXZ+0.80,PYZ+0.4)
320 CONTINUE
310 CONTINUE
300 CONTINUE
CALL EXIT
END

```

VARIABLE ALLOCATIONS

R(R))=0000	XSCAL(R))=0002	YSCAL(R))=0004	XO(R))=0006	YO(R))=0008	SQ(R))=000A
SMSQ(R))=000C	FZ(R))=000E	XHZS(R))=0010	XKZS(R))=0012	XLZS(R))=0014	X11(R))=0016
X12(R))=0018	X13(R))=001A	XZ1(R))=001C	XZ2(R))=001E	XZ3(R))=0020	X31(R))=0022
X32(R))=0024	X33(R))=0026	S1(R))=0028	S2(R))=002A	S3(R))=002C	A11(R))=002E
A12(R))=0030	A13(R))=0032	A21(R))=0034	A22(R))=0036	A23(R))=0038	A31(R))=003A
A32(R))=003C	A33(R))=003E	XHZ(R))=0040	XKZ(R))=0042	XLZ(R))=0044	X11(R))=0046
X12(R))=0048	FX1(R))=004A	AZ(R))=004C	GAMZ(R))=004E	TANZ(R))=0050	SQRA(R))=005
FZ1(R))=0054	PX2(R))=0056	PYZ(R))=0058	AXLZ(R))=005A	APXZ(R))=005C	APYZ(R))=005E
HZ1(R))=006A	HZ1(R))=0068	HZ1(R))=006C	HZA(R))=006D	KZ1(R))=006E	KZ1(R))=006F
LZ1(R))=0070	LZ1(R))=0071	KZA(R))=0072	LZA(R))=0073	IH(R))=0074	IF(R))=0075
IK(R))=0076	IK1(R))=0077	IL(R))=0078	IL1(R))=0079	N(R))=007A	KZ1(R))=007B

02 JAN 70
PAGE 004

LZ111(1)=007C

STATEMENT ALLOCATIONS

390 =00B3	391 =0086	329 =011F	351 =0126	301 =0234	344 =0285	343 =0280	342 =02C2	340 =02C2
354 =02EA	352 =02F5	353 =02FE	356 =0302	355 =0328	359 =0340	357 =034C	358 =0365	324 =036C
325 =0399	361 =03BF	360 =03EA	371 =03F0	370 =041C	381 =0421	326 =044F	366 =04A1	376 =04A1
375 =04D2	386 =04D7	320 =0503	310 =050C	300 =0515				

FEATURES SUPPORTED

TRANSFER TRACE
ARITHMETIC TRACE
ONE WORD INTEGERS
IOCS

CALLLED SUBPROGRAMS

SCALE	FSORT	IABS	FATAN	FSIN	FCOS	FABS	FPLT	PRINT	FCAR	FAD	FSUB	FMPY	FDIV	FLD
FSTO	FSRR	FOVR	FAXI	MFAR	MTAR	FLOAT	MTIF	MTIF	HWRT	MCOMP	MTOT	SNR	FCRRI	HOLEB
PRNTN	EBPRT	CARDN												

REAL CONSTANTS

.110000E 02=007E	.390C00E 00=0080	.000000E 00=0082	.400000E 01=0084	.500000E 00=0086	.100000E 01=0088
.100000E 05=008A	.100000E 03=008C	.314193E 01=008E	.200000E 01=0090	.785398E 00=0092	.100000E 00=0094
.600000E-01=0096	.120000E 00=0098	.157100E 01=009A	.400000E 00=009C	.400000E-01=009E	.240000E 00=00A0
.250000E 00=00A2	.550000E 00=00A4	.800000E 00=00A6	.300000E-01=00A8		

INTEGER CONSTANTS

7=00AA	17=00AB	9=00AC	1=00AD	5=00AE	2=00AF	8=00B0	0=00B1	11=00B2
--------	---------	--------	--------	--------	--------	--------	--------	---------

CORE REQUIREMENTS FOR PROG

COMMON	0	INSKEL COMMON	0
VARIABLES	126	PROGRAM	1186

END OF COMPILATION

Chapter 2

ELECTRICAL CHARACTERIZATION OF QUASI MOS STRUCTURES ON SILICON

by

W. R. Fahrner, E. F. Gorey, and C. P. Schneider

INTRODUCTION

Junctions are present in important devices, e.g., in buried-channel charge-coupled devices (CCDs) or in silicon on sapphire (SOS)-based integrated circuits. In order to optimize the performance of such a device--speed, transfer efficiency, etc.--the characterization of the electrical properties of the material is desirable. For homogeneous silicon, there are some standard techniques based on metal oxide semiconductor (MOS) capacitance measurements for this purpose. The presence of underlying junctions requires important precautions to be made with the use of MOS-CV measurement techniques.

Owing to the junction, the number of components of the equivalent network increases and the analysis is impeded. It will be shown in this paper how this problem can be solved. When one side of a junction described above is oxidized, a quasi MOS structure results. The equivalent network of such a structure is discussed in this paper, and the conditions for MOS C-V and G-V measurements are given. In the case where the MOS admittance can be measured, the following information can be obtained:

1. The surface-state density N_{ss} (1), the corresponding capture cross sections (2), the charge density in the oxide (3), and deep energy levels (4).
2. The doping concentration N_D .
3. The lifetime of the minority carriers (5).

Measurements on epitaxial junctions according to (3) have already been carried out (6) without an adequate theoretical basis.

In this investigation, we are primarily interested in the measurement of lifetime, since this parameter is more sensitive to defects and impurities in the crystal than any other electrical parameter (7). Thus, in the section "Range of Quasi MOS Capacitance Technique," the values for layer and substrate resistivity, dot diameter, oxide thickness, etc., refer to ranges in which such lifetime measurements can be carried out.

ANALYSIS OF EQUIVALENT NETWORK

In Fig. 1, a cross section of an oxidized n epitaxial layer on a p^- substrate is shown. The network of the structure consists of the oxide capacitance C_{ox} , the distributed layer resistance R of the n-layer, the distributed junction admittance $Y_J = G_J + j\omega C_J$, and the distributed substrate resistance R_s . A net consisting of buried layers each of 2.5 times 2.5 mm² area with a spacing of 8 mm is diffused into the substrate prior to epitaxy. The doping profiles underneath A (off the

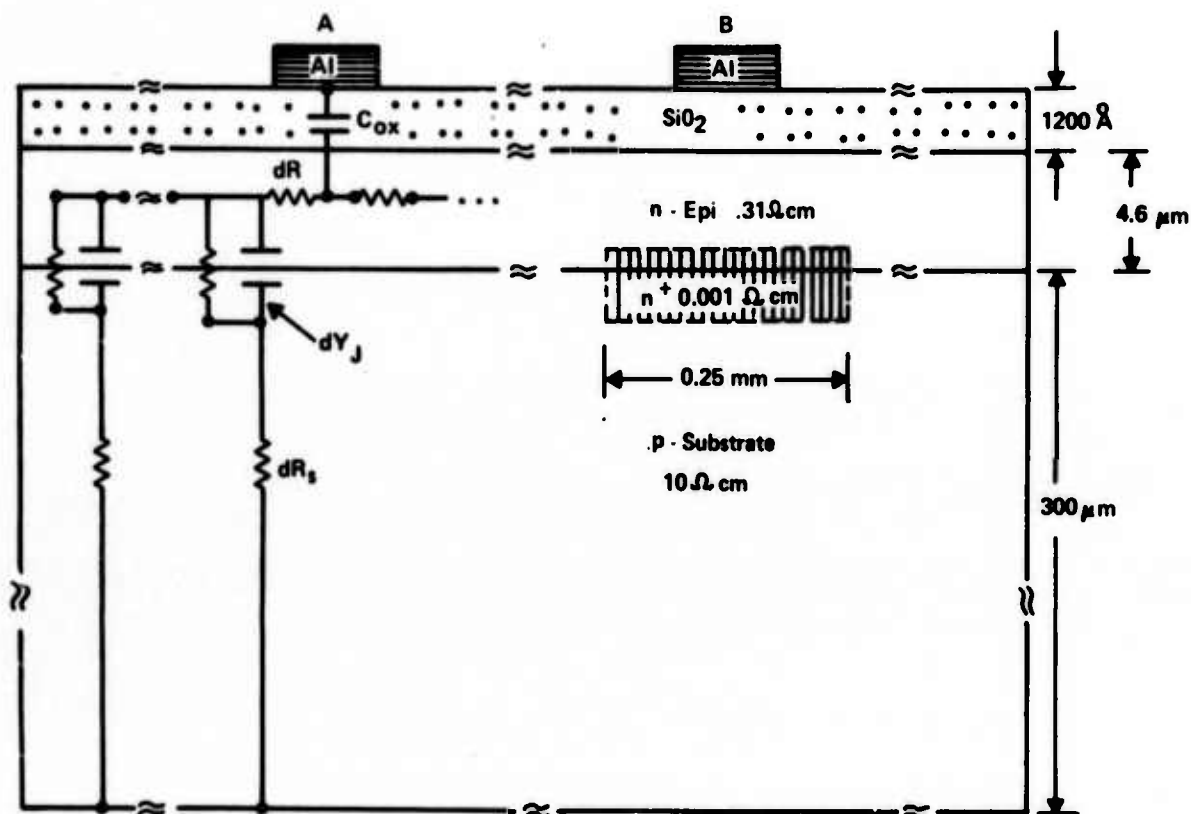


Fig. 1. Cross section of a n-p⁺ junction. The n layer was grown by regular gas phase epitaxy. It is covered by 1200 \AA thermal oxide.

buried layer) and B (on the buried layer) are obtained by the spreading resistance technique (Fig. 2). The C-V curves for two dots off the buried layer are shown in Fig. 3. The dots have areas of 0.01765 and 0.00196 cm². The same measurements are repeated for a <115> and a <100> oriented wafer with epitaxial layer resistivity of approximately 0.9 ohm-cm and of approximately 4-μm epitaxial thickness. The substrate resistivity is 8 and 6 ohm-cm respectively (Fig. 4a,b). In these wafers, no buried layer is present.

The analysis of the data given in Fig. 3 reveals that the measured low-frequency capacitance in accumulation is identical with the oxide capacitance. This is confirmed through measurements on control wafers, by measuring the oxide thickness and the capacitances for different dot areas and comparing the ratios with the area ratios.

The dc voltage drop (v_J) across the junction is 0 since there is no dc current flow through the MOS structure.

The ac admittance is given by $G_J(v_J) + j\omega C_J(v_J)$ with $v_J = 0$. G_J can be derived as $G_J = dI_J/dv_J = I_0 \times (q/kT) \times \exp(qv_J/kT)$. In anticipation of the results, the lifetime of the epitaxial layer (which is heavily doped compared with the substrate and can be expected to give the major contribution to the dark current) is measured now to be approximately 1 μsec. With this

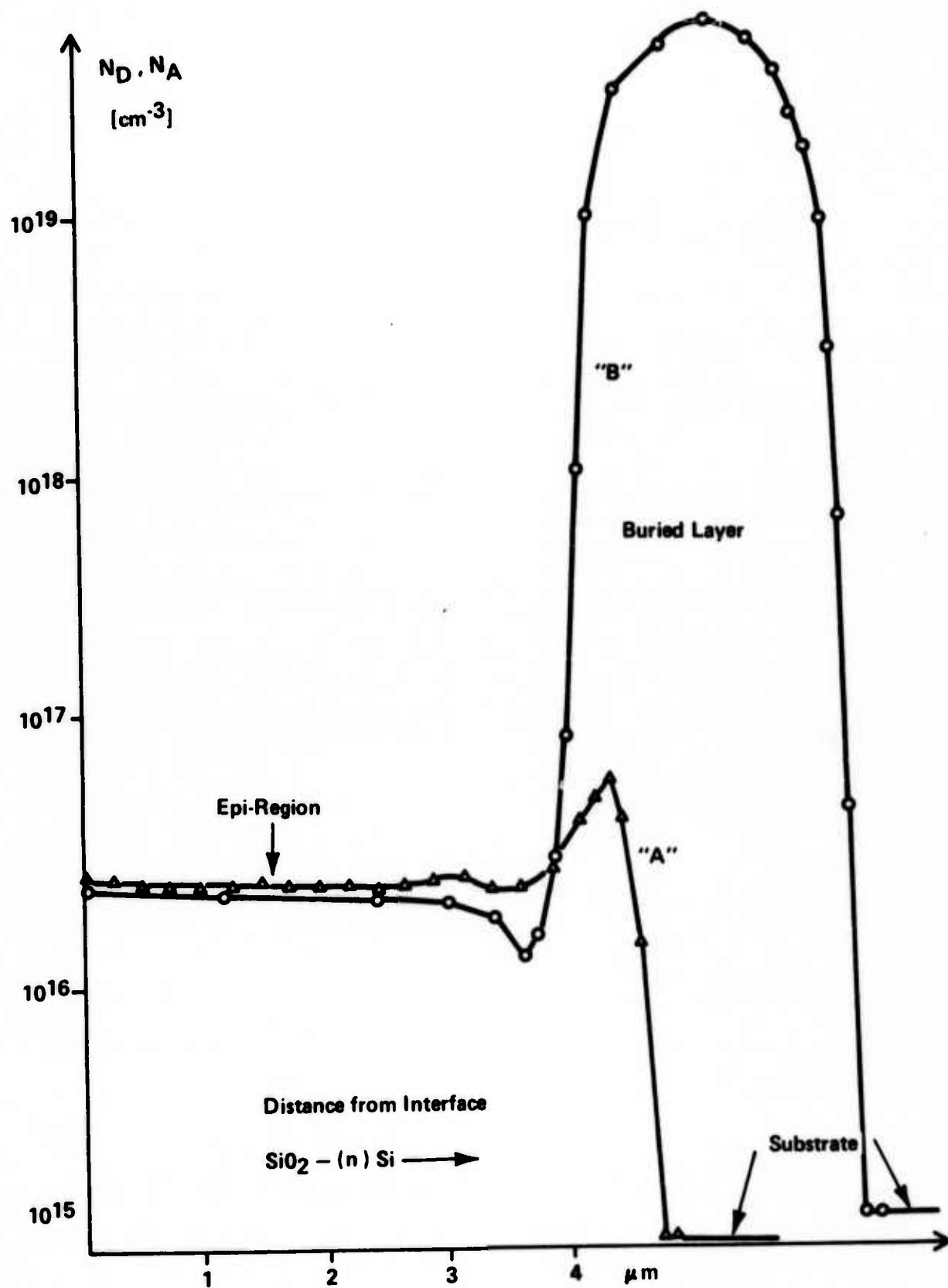


Fig. 2. Doping profiles underneath the dots A (triangles) and B (circles) in Fig. 1.

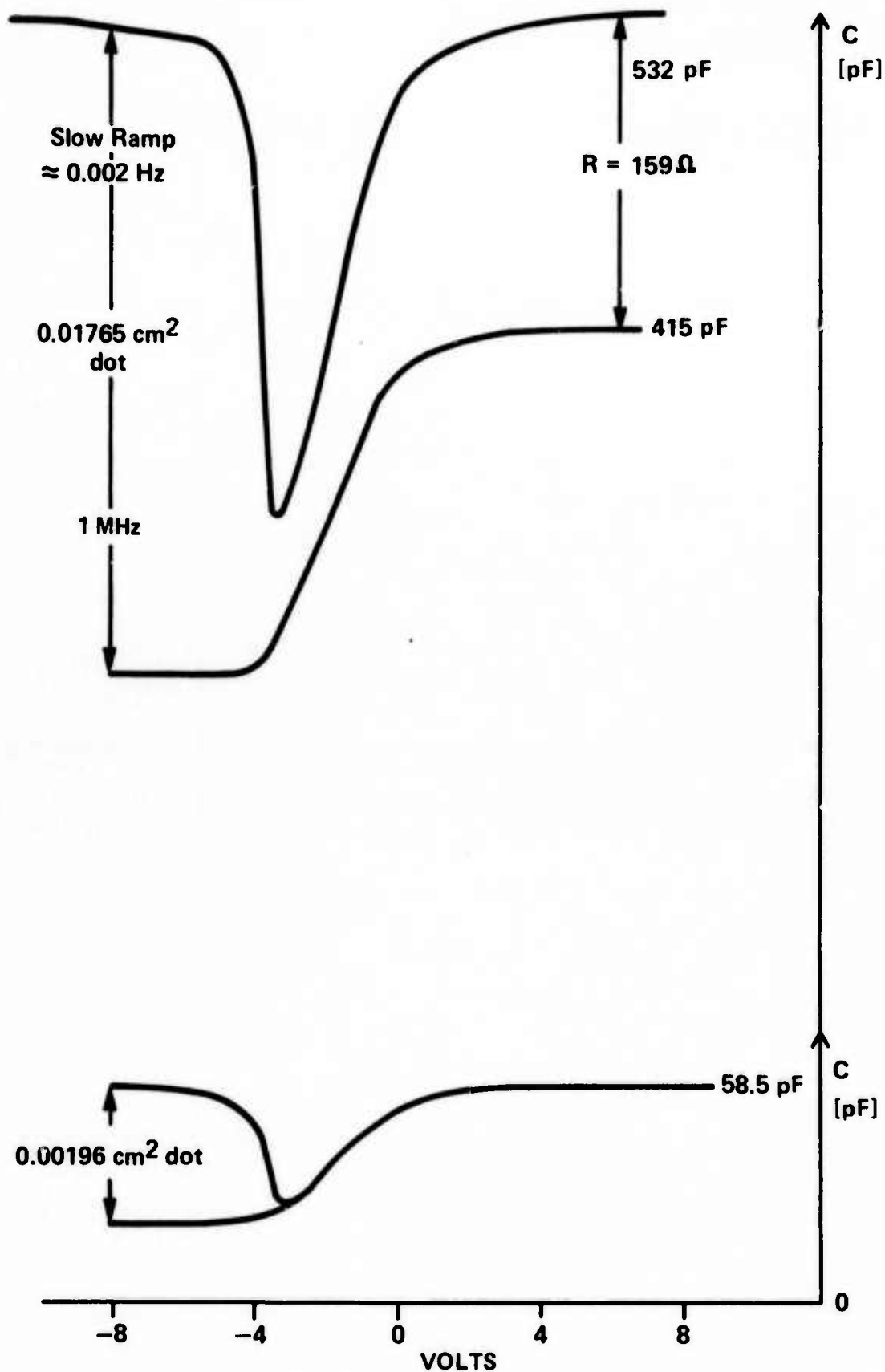


Fig. 3. C-V curves for two dots off the buried layer (A in Fig. 1).
Note that for the smaller dot no dispersion is seen.

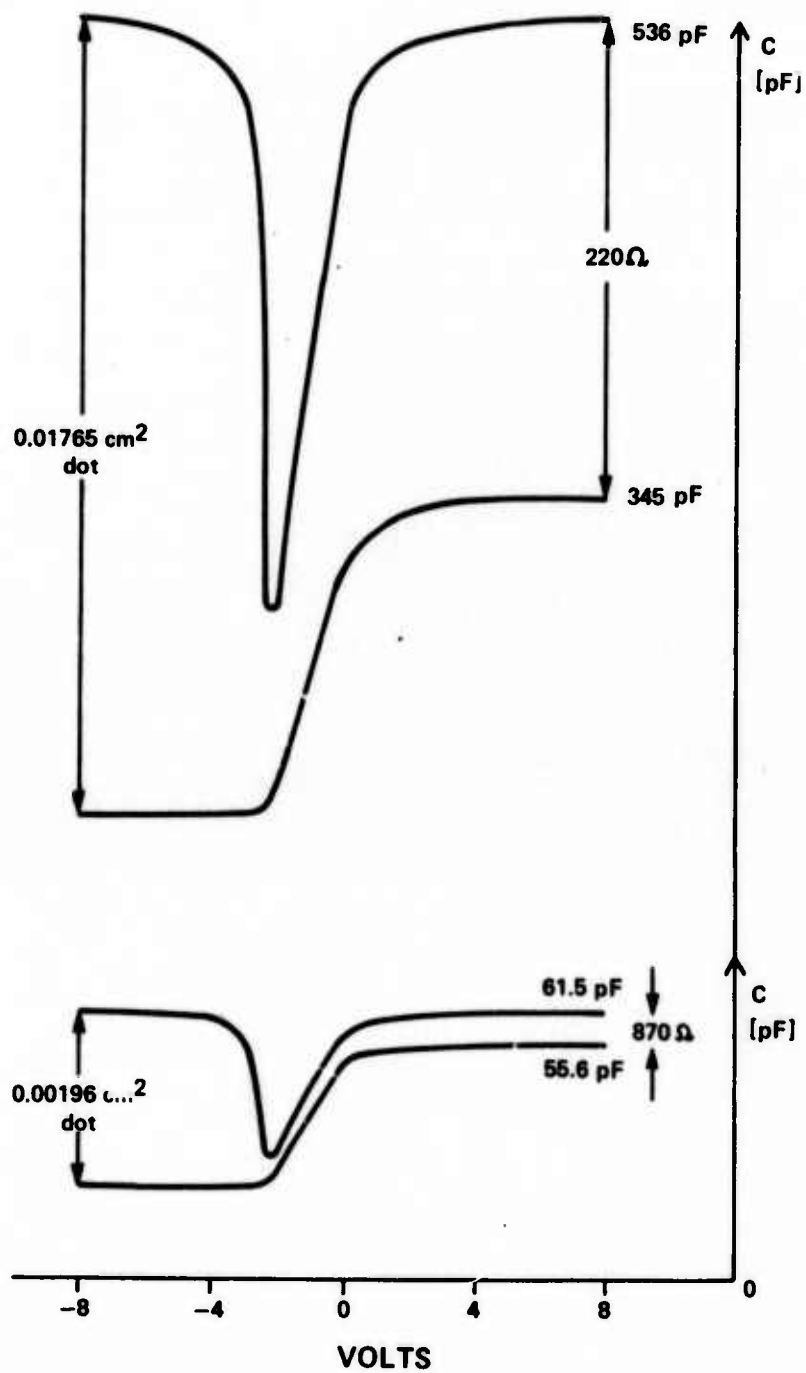


Fig. 4a. The same C-V curves as in Fig. 3 for a $\langle 115 \rangle$ oriented substrate wafer. The epitaxial resistivity is three times larger than that in the samples characterized in Fig. 3.

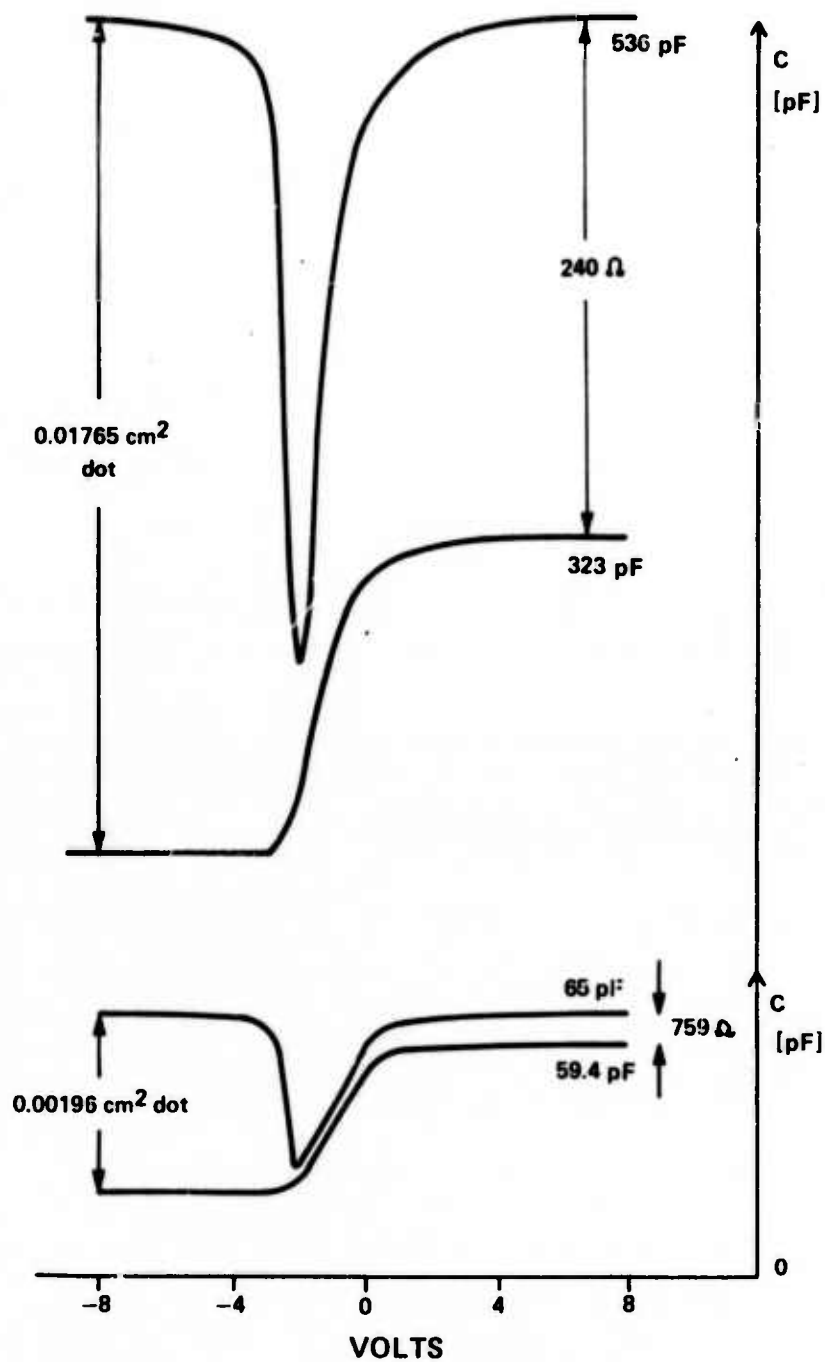


Fig. 4b. The same C-V curves as in Fig. 3 for a '100' oriented substrate wafer. The epitaxial resistivity is three times larger than that in the samples characterized in Fig. 3.

value and the given wafer data, one obtains $I_o \sim 10^{-9}$ A, and thus $G_J \sim 4 \times 10^{-8} \exp(qv_J/kT)$ mhos. The capacitance C_J is ~ 20 nf at 0 Volt and $\omega C_J \sim 10^{-10}$ mhos for a frequency of 2×10^{-3} Hz. (I_o and C_J have been calculated by means of Shockley's equation $I_o = qA (p_n \sqrt{D_p/\tau_p} + n_p \sqrt{D_n/\tau_n})$ and the depletion approximation $C_J = \epsilon A \left(\frac{q}{2\epsilon v_D} \cdot \frac{N_D \cdot N_A}{N_D + N_A} \right)^{1/2}$. v_D is the diffusion potential. The other symbols have the usual meaning.) The ac admittance is resistance-controlled up to ~ 1 Hz. Even in range $f > 1$ Hz, there is no influence of the junction admittance, since $\omega C_J \gg \omega C_{ox}$. These considerations explain why a voltage-independent accumulation capacitance is measured over the usual frequency and bias range. The validity of the assumption on $G(v_J)$, $C(v_J)$, and the numeric values are found in good agreement with $C(v_J)$ and differentiated $I(v_J)$ curves measured after oxide removal and ultrasonic cutting (e.g., $C_J = 35$ and 40 nf for dots cut at A and B, respectively).

The bulk resistance R_s of the substrate can be neglected as long as the resistivity is not too large. Experimentally, the upper limit was found to be approximately 50-100 ohm-cm and is theoretically given by the comparison of the RC_{ox} time constant with the measurement frequency of 1 MHz.

From the data given in Fig. 3 (i.e.: $C_{ox} = 532$ pf, $C_{HF}(\text{acc.}) = 415$ pf), the lumped series resistance can be determined:

$$C_{HF} \text{ (acc)} = C_{ox} / (1 + \omega^2 \tau^2) \quad [1]$$

$$\tau = RC_{ox} \quad [2]$$

This gives $R = 159$ ohms. For the case of a buried layer underneath the dot, this value is reduced to $R = 88$ ohms. (Note that in Fig. 2 the buried layer extends into the epitaxial layer due to outdiffusion.) When the dot area is reduced to 0.00196 cm^2 and the capacitance to 58 pf , no dispersion is observed in accumulation up to 1 MHz . With the same values of R , one obtains now $(\omega\tau)^2 = (2\pi \cdot 10^6 \cdot R \cdot C_{ox})^2 = 3.4 \times 10^{-3}$ and 1×10^{-3} , respectively; C_{ox} can be measured with 1 MHz .

Since the time constant of the surface states is usually observed in the kHz range, $G(V)$ and $G(\omega)$ measurements (2) are also feasible. (A $G(V)$ and a $G(\omega)$ curve is a plot of the total conductance G vs voltage or frequency at a fixed frequency or voltage respectively.) This is roughly checked by measuring $G(V)$ in the kHz range. The typical peak due to surface states and its shift with frequency is observed.

From Fig. 4, one obtains R values of 220 ohms and 240 ohms for $N_D = 5 \times 10^{15}$ and $4.8 \times 10^{15} \text{ cm}^{-3}$, respectively.

SPREADING RESISTANCE VS DOT DIAMETER

For frequencies $\omega \leq 1/RC_{ox}$, the equipotential lines of the structure are schematically drawn in Fig. 5a. Therefore, one can assume a disk-like volume representing the epitaxial layer, in which the current flows (Fig. 5b). The voltage v_o is applied at the inner area $2\pi r_o \cdot d_{epi}$, d_{epi} being the epitaxial layer thickness; the outer area at r_1 is grounded. A voltage dv drops across a volume increment $2\pi r dr \cdot d_{epi}$:

$$dv = -i_o dR$$

(i_o is the current caused by v_o).

dR is defined by

$$dR = \rho \cdot dr / A(r) = \rho \cdot dr / (2 \cdot \pi \cdot r \cdot d_{epi})$$

$$dv = -i_o \cdot \rho \cdot dr / (2 \cdot \pi \cdot r \cdot d_{epi})$$

$$v = - (i_o \cdot \rho / 2 \cdot \pi \cdot d_{epi}) \ln (r/r_1).$$

Since $v(r_o) = v_o$:

$$(v_o/i_o) = R = - (\rho/2 d_{epi}) \ln (r_o/r_1) \quad [3]$$

As a result, one obtains an increase of the spreading resistance for smaller dot diameters. For the epitaxial wafers of Figs. 2 and 3, we are not able to observe this change, first because the spreading resistance is too small, second, because the existence of the junction and oxide capacitance heavily interferes with the assumption of a simple radial current. For the SOS wafers shown here, however, the effect is clearly visible. For an oxide of 1300 Å, and an $\sim 10\text{-}\mu\text{m}$ -thick epitaxial layer of 1 ohm-cm, one obtains $R = 500, 1380,$ and ~ 2450 ohms for dots of 0.01765, 0.00196, and 0.00049 cm²,

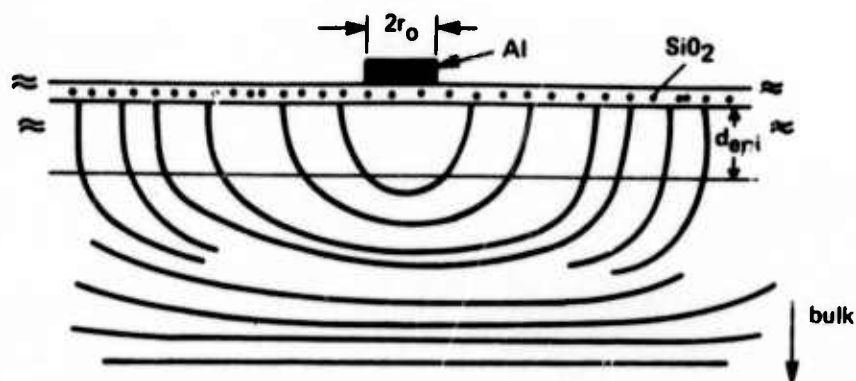


Fig. 5a. Equipotential lines for frequencies $\ll 1$ MHz. The current flow in the epitaxial layer is practically radial.

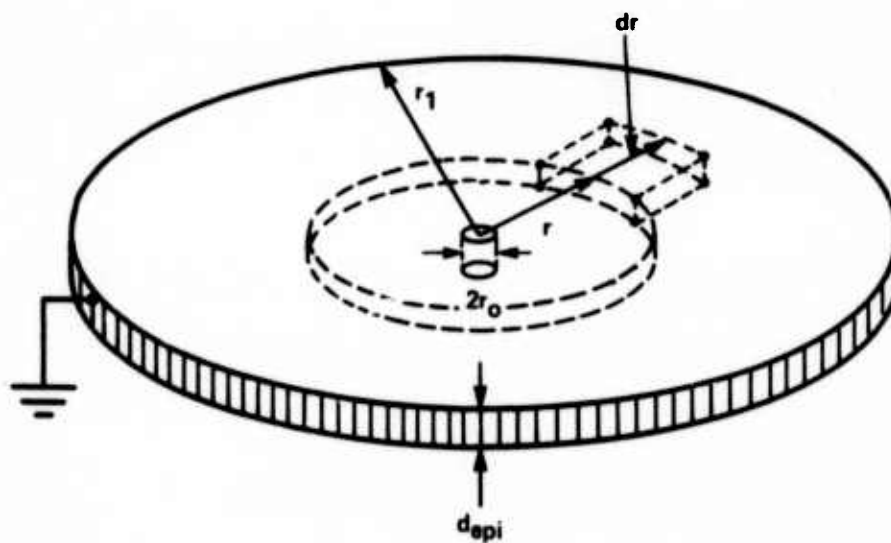


Fig. 5b. The epitaxial layer in a simplified disk-like geometry. For $r < r_0$, the potential is assumed to be constant ($= v_0$).

respectively. Since, for these structures, contact with the backside is made by overlapping Al at the edge of the wafer, the spreading resistance is measured without distortion by the junction capacitance. Though we do not observe an $R \propto (-\ln r_0)$ dependence but, rather, an $R \propto 1/r_0$ one, the model qualitatively describes the behavior of the spreading resistance.

RANGE OF QUASI MOS CAPACITANCE TECHNIQUE

In the preceding sections, we have shown that the contribution of the junction impedance can be neglected, if appropriate values for the resistivities, oxide thickness, dot diameter, etc., are selected. In the following, we give approximate ranges for those parameters. Within these ranges, the junction impedance is small compared with the interface, oxide, and layer impedance.

For a 5- μm layer of $\rho \sim 0.3$ ohm-cm resistivity and 1200 Å SiO_2 , a dot of $d \leq 0.5$ -mm diameter should be used. The substrate might have $\rho \leq 20$ ohm-cm. For other oxide thicknesses d_{ox} , d can be chosen to be $d = \frac{0.5}{1200} d_{\text{ox}}$. For higher layer resistivities, the layer thickness should be increased according to the resistivity ratio. For epitaxial ρ values ≥ 15 ohm-cm, care must be taken that the condition $C_{\text{ox}} \ll C_J$ is still valid, e.g., by increasing the wafer area. For the insulator-silicon structure, with an oxide thickness of 1300 Å and a layer of

$\sim 10 \mu\text{m}$ and $N_D, N_A \sim 1-2 \times 10^{16} \text{ cm}^{-3}$, we consider a dot of 0.25-mm diameter as appropriate. The same changes in dot diameter and epitaxial layer thickness should be done for a variation in oxide thickness and layer resistivity. The diameter of the wafer should be at least 1-1/4 inches. Since these values refer to the oxide capacitance ($\tau = RC_{ox}$) and the lifetime measurements are carried out with the inversion and deep depletion capacitance (8), the accuracy increases by $(C_{ox}/C_f)^2$. (Cf. Eq. [1].)

COMPARISON WITH OTHER TECHNIQUES

Finally, this technique should be compared with some alternatives, namely, the MOS emitter device and the buried-layer SOS structure, described, for example, in Refs. (9) and (10). Though some restricting conditions are implied in our technique, such as dot diameter, epitaxial layer thickness, etc., its advantages are greater versatility and measurement without distortion of a conduction layer. For example, the technique of Jones and Barber (9) is restricted to lifetimes, whereas a buried conduction layer (10) might cause out-diffusion and thus a reduction of lifetimes even in the epitaxial bulk.

Measurements using a guard ring as a counterelectrode were made. The substrate was at the same potential as the guard ring. The equivalent network consists of the oxide and space charge capacitance, C_{ox} and C_{sc} , respectively, of the dot

in series with the oxide capacitance C_{oxR} , the space charge capacitance C_{scR} of the ring, and the spreading resistance of the layer. The network is shunted by the coupling capacitance C_c between the dot and the ring. (We neglect here the shunt to the substrate, because this has been discussed above.) The condition $C_{ox} \ll \frac{C_{oxR} \cdot C_{scR}}{C_{oxR} + C_{scR}}$ can be fulfilled by the appropriate choice of the ring area. The condition $C_c \ll \frac{C_{ox} \cdot C_{sc}}{C_{ox} + C_{sc}}$ is always valid since oxide thicknesses of 500...5000 Å are used. For a dot diameter of 60 mils, an oxide of 1000 Å, and a spacing of 150 μm, one obtains $C_c = 10^{-4}$ pf. Thus dispersion-free C-V curves are feasible. This was confirmed by the experiment. However, a disadvantage is encountered: with the present state of the art, photoresist deteriorates the oxide and silicon properties, especially the lifetimes and the oxide stability. We observed reductions in lifetimes from 500 μsec to 0.1 μsec and flatband shifts. (The lifetime data of the paper were obtained by the technique given in Ref. 8.)

RESULTS AND DISCUSSION

The results of the measurements can be summarized as follows: Flatband voltages and surface-state densities are found in the usual ranges of $\sim -1V$ and $\leq 1.4 \times 10^{10} \text{ eV}^{-1} \text{ cm}^{-2}$, respectively.

Since the peak of the G-V curves is found at depletion surface potentials for frequencies in the kHz range, the capture cross section can be expected to be 10^{-13} to 10^{-15} cm². No deviation compared with "normal" MOS structures can be seen. Lifetimes are measured to be 1 μsec in the epitaxial wafers, 10^{-3} μsec in the n-SOS wafers, and 0.1 μsec in the p-SOS wafers.

The SOS low-frequency curves for wafers of layer thicknesses between 1 and 10 μm do not show any trace of a donor or an acceptor level (Fig. 6). This is in contradiction to earlier reports (11, 12), where an acceptor and a donor level at $E_c - E_A = 0.25$ eV and $E_D - E_v = 0.30$ eV were published. This might be attributed to different measurement techniques. The densities of the levels are reported to be 10^{17} to 10^{18} cm⁻³. A good resolution for surface states (or bulk impurities seen as surface states) for the slow ramp technique is 10^{11} cm⁻². If this value is divided by an effective distribution width of 10 to 100 Å, one obtains bulk concentrations of 10^{17} to 10^{18} cm⁻³. The slow ramp technique, however, measures states localized at the surface, whereas the techniques used in Refs. (11) and (12) cover the total depth of the film. Thus, it might be concluded that the reported levels are located near the Si-Al₂O₃ interface.

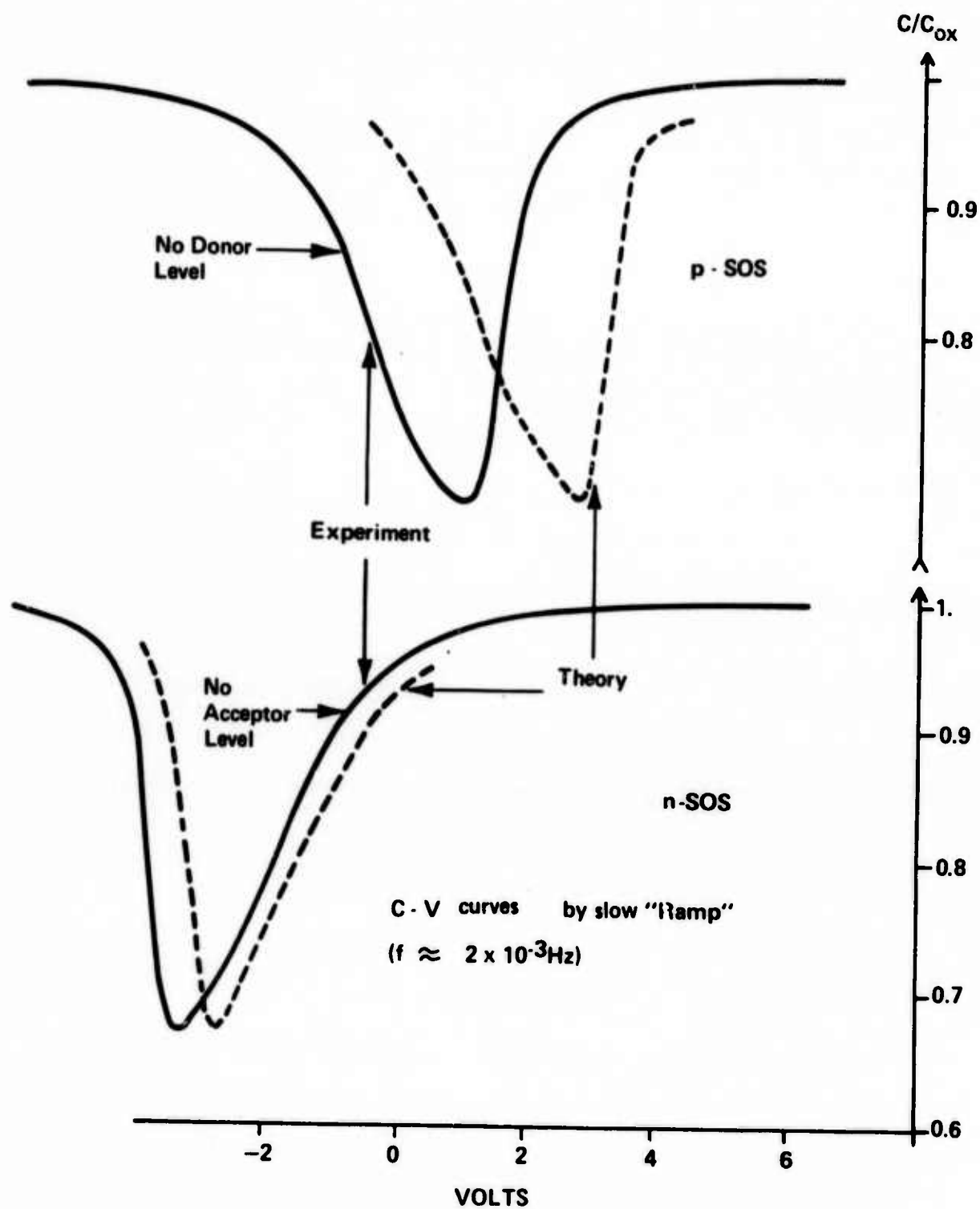


Fig. 6. Enlarged portion of the low frequency C-V curve of a p- and an n- SOS wafer. No indication of a deep lying level is visible. For comparison, the ideal low frequency curves are shown too.

Another possible explanation is the fact that one deals with extremely deep levels. Their time constant is controlled by the surface potential u_s :

$$\tau_p = (\sigma \cdot v_{th} \cdot N_A)^{-1} \exp(-u_s)$$

Since the levels are defined to be either acceptor or donor levels, they exchange carriers only with the valence or conductance band, respectively. With the given data and an assumption of a capture cross section $\sigma = 10^{-15} \text{ cm}^2$ and a thermal velocity $v_{th} = 10^7 \text{ cm/sec}$, one obtains for the hole dispersion time constant in the n-type wafer $\tau_p = 2 \times 10^2 \text{ sec}$. This value is comparable to our measurement frequency of $2 \times 10^{-3} \text{ Hz}$. Capture cross sections of 10^{-15} cm^2 have been measured (13); in this case, however, higher values are more likely, and the first explanation should be preferred.

SUMMARY AND CONCLUSIONS

The measurement of the admittance of an MOS structure over a p-n junction or on SOS devices is discussed. It is shown that by appropriate choice of the wafer data, the contribution of the junction to the total admittance can be neglected and lifetime measurement can be carried out.

No deep levels can be seen for the SOS system.

REFERENCES

1. R. Castagne, C. R. Acad. Sc. (Paris), 267, Serie B, 866 (1968).
2. E. H. Nicollian and A. Goetzberger, Bell System Tech. J., 46, 1055 (1967).
3. D. R. Kerr, Int. Conf. on Properties and Use of MIS Structures, J. Borel, Editor, CNRS-LETI, Grenoble, 303 (1969).
4. W. R. Fahrner and A. Goetzberger, Appl. Phys. Lett., 21, 329 (1972).
5. M. Zerbst, Z. Angew. Phys., 22, 30 (1966).
6. P. Rai-Choudhury and D. K. Schroder, J. Electrochem. Society, 119, 1580 (1972).
7. Technical Report No. 4.
8. W. R. Fahrner and C. P. Schneider, ESSDERC, Nottingham, England (1974).
9. J. E. Jones and H. D. Barber, IInd Int. Symp. on Silicon Materials Science and Technology, March 13-18, Chicago, 561 (1973).
10. D. K. Schroder and P. Rai-Choudhury, Appl. Phys. Lett., 22, 455 (1973).
11. F. P. Heiman, *ibid.*, 11, 132 (1967).
12. D. J. Dumin, Solid-State Electron., 13, 415 (1970).
13. W. Fahrner and A. Goetzberger, Appl. Phys. Lett., 17, 16 (1970).